International Journal of Adhesion & Adhesives 142 (2025) 104089

Contents lists available at ScienceDirect

International Journal of Adhesion and Adhesives

journal homepage: www.elsevier.com/locate/ijadhadh

A two-step full laser surface treatment to improve the adhesive bonding of aluminium-aluminium joints

Davide Morello [a], Claudio Leone [a,c,*], Giuseppe Lamanna [a], Genna Silvio [b,c]

[a] University of Campania Luigi Vanvitelli, Department of Engineering, Via Roma 29, 81031, Aversa, CE, Italy
[b] University of Rome Tor Vergata, Department of Enterprise Engineering, Via del Politecnico 1, 00133, Rome, Italy
[c] CIRTIBS Research Centre, University of Campania Luigi Vanvitelli, Via Roma 29, 81031, Aversa, CE, Italy

ARTICLE INFO

Keywords:
Laser texturing
Laser cleaning
Surface preparation
Adhesive joining
Aluminium alloy

ABSTRACT

To improve the adhesion between Aluminium-Aluminium joints, a two-step laser surface treatment was developed and tested, adopting a 30W pulsed Yb:YAG nanosecond laser source. The process consists of a first phase, called laser texturing, where a deep texture is obtained on the adherents by adopting high pulse energy and several repetitions, followed by a further laser treatment, called laser cleaning, carried out with lower energy content, and applied over the overall adhesion surface. To characterise the treatment process, the effects of technological parameters on texturing geometry were first investigated to select the proper texture; then, textures with different selected geometries were carried out and adopted to produce single-lap joints according to the ASTM D1002-10 Standard. An epoxy system adhesive was adopted for the joining. Furthermore, samples with only one-step treatment (i.e. only laser texturing or laser cleaning), standard treatment (sandpaper), and acetone cleaning were fabricated and adopted as reference samples. Analysis of variance was applied to study the effect of the process parameters, and digital image analysis was adopted to evaluate the percentage of adhesive/cohesive failure. From the results, compared to the only textured reference samples, the two-step laser treatment increases the apparent shear stress regardless of the adopted texture geometry. Moreover, it was found that only laser cleaning treatment can significantly improve joint strength compared to the untreated sample.

1. Introduction

Thanks to their high strength-to-weight ratio, ease of fabrication, excellent thermal conductivity, high corrosion resistance and attractive appearance at their natural finish, aluminium alloys are widely used in several industrial applications, including aerospace, automotive and structural architecture [1–5]. In these industrial fields, assembling components with complex geometries and shapes is critical for achieving the desired structural performance and durability of the product/components. Consequently, assembly techniques must withstand significant loads to maintain the design requirements and the structural integrity. Mechanical joining techniques, such as riveting, bolting, and welding, are commonly adopted due to their ease of application, good mechanical properties, and well-known behaviour. However, these methods can induce local stress concentrations and modify the metallurgical properties of the materials [5–7]. The adoption of adhesive in place of traditional joining techniques is very attractive in structural design since the former offers several advantages, including uniform stress distribution, weight reduction, vibration attenuation, acoustic insulation, and corrosion resistance [8,9]. However, surface preparation is mandatory to achieve maximum bonding strength and durability when bonding with adhesives [3,4]. To improve the adhesion, mechanical treatments, such as sandblasting, grit blasting, machining, rolling and micro discharge machining, are adopted to increase the bonding area and its surface roughness, while chemical treatments and anodization methods modify surface wettability and chemistry [10–15]. Generally speaking, mechanical treatments increase the effective bonding area and promote mechanical anchoring, while chemical treatments remove contaminants and promote adhesion by changing the chemical affinity [8]. However, mechanical and chemical treatments have several drawbacks: the treatment area cannot be accurately defined; sand/grit blasting can leave contaminants trapped in the material; the processes involve multiple steps and long processing times; they have environmental impacts and generate costly waste; and they pose safety risks for workers [8,16,17].

Laser treatments have emerged as a promising alternative to

* Corresponding author. University of Campania Luigi Vanvitelli, Department of Engineering, Via Roma 29, 81031, Aversa, CE, Italy
E-mail address: claudio.leone@unicampania.it (C. Leone).

https://doi.org/10.1016/j.ijadhadh.2025.104089
Received 12 February 2025; Received in revised form 4 June 2025; Accepted 16 June 2025
Available online 18 June 2025

mechanical and chemical surface preparation methods for adhesive joints [18]. More in detail, laser texturing and laser cleaning treatments are becoming increasingly popular for the preliminary preparation of adhesive joints between homogeneous or non-homogeneous materials [18–20]. The former refers to a process where a laser beam is adopted to obtain dimples or grooves with different geometries and configurations (lines, grid, etc.), useful to increase the apparent surface and generate mechanical interlocking. The latter comprises a family of advanced surface treatments that adopt short or ultra-short pulsed lasers to peel off, vaporise, sublimate, or burn away unwanted material without causing specific harm to the substrate. Laser cleaning is used in several applications to remove unwanted surface materials like coatings [21], paints [22–25], rust [26,27], and oil [28], or before welding [29,30], coating [31,32], and bonding [7,33] for surface preparation. Moreover, by appropriate laser parameter settings, the treatment allows the surfaces' micro or nano-texturing [25,34,35], providing a better grip for adhesive areas and frictional and form-locking connections. Laser texturing/cleaning offers several advantages compared to mechanical or chemical treatments. These include the absence of mechanical contact and tool wear, independence from material hardness, and the ability to treat complex surfaces with high precision (i.e. a clear definition of the treated and untreated areas). The thickness of the removed layer (e.g., rust, paint, or contaminants) can be precisely controlled by adjusting process parameters. In addition, laser processes are easy to automate, environmentally friendly, and, with proper precautions, safe for workers. Texture patterns can also be easily modified using CAD/CAM software [6,7,36]. These advantages make laser treatment an emerging and attractive technology for industrial applications. Furthermore, the availability of short and ultrashort laser sources with high average power (up to 500W) significantly reduces the treatment times, enhancing their industrial viability.

An in-depth analysis of the influences of laser process parameters and texturing geometry on the bonding strength is necessary to improve the adhesion. Recent studies examined various surface preparation techniques and texturing to enhance adhesive bonding on similar and dissimilar material joints [37–41]. Laser treatments have enabled control of the surface roughness at macro and micro levels, surface adhesion area, and wettability, so that an appropriate selection of laser parameters and texturing geometries can significantly increase the adhesive bonding.

In [42], laser surface texturing was investigated as a method to enhance the adhesive bonding of Ti6Al4V alloy. Three different textures were created using a 50W fiber laser with a pulse length of 100 ns, and their effect was evaluated using a lap shear test. Results showed significant improvement in the bonding strength of the laser-treated surface compared to the sand-blasted one. However, it was found that the failure mode depends on the texture type: partial cohesive for dimples, fully cohesive for the grid, and textured substrate failure for chaotic patterns. Similarly, in Ref. [43], sandpaper, acid etching, and laser texturing were compared as surface preparation techniques before bonding the Ti6Al4V alloy. It was found that laser texturing resulted in higher bonding strength than all the other methods tested, with an increase of up to 4.5 % over sandblasting. In Ref. [44], four methods (P180 sandpaper, Scotch-Brite, laser cleaning, and laser texturing) were applied to aluminium alloy EN AW-5754 and stainless steel X5CrNi18-10 using three types of epoxy adhesives. Results indicated that laser cleaning provided the highest shear strength for aluminium, with cohesive failure observed depending on the adhesive type. G. Li et al. [45] compared sandblasting and laser ablation on aluminium alloy, analysing the effects of laser spot distribution on surface roughness, contact angle, chemical composition, and shear strength. Results showed that the bonding performance can be improved by adopting an optimal laser spot that induces micro-nano composite structures, which increase contact area and shear strength. Therefore, it is important to analyse the effects of laser process parameters on the texturing geometry, as it has emerged as the predominant factor influencing adhesion. In Ref. [6], the authors explored the impact of laser micromachining of crater-array and multi-grooves on the bonding strength and failure mode of 7075-T6 aluminium alloy adhesive joints. They propose a two-step laser processing method to enhance the shear strength, consisting of an initial crater array followed by a groove pattern. Findings revealed that using parallel grooves with 100 μm spacing, and a scan number equal to 2, increased the shear strength up to four times. This behaviour was confirmed in Ref. [46], where the authors explored different laser texturing methods to enhance the adhesion performance and corrosion resistance of AA7075-T6 bonded joints. The optimal adhesion was achieved by adopting a parallel grooves pattern placed perpendicular to the load application (Hatch distance = 60 μm) and in a box-type configuration. These designs effectively shifted failure modes from mixed to cohesive, improving adhesion performance even after corrosion exposure. Although the possibility of improving the bonding strength by adopting the multi-groove pattern, the groove distance (Hatch Distance, Hd) is a key parameter to avoid adhesive failure. When Hd is too large, the amount of non-treated area increases; consequently, the adhesion failure mode prevails, resulting in a decrease in bonding strength. These findings were analysed and improved in Ref. [47], where three different microstructures (a crater array, multi-groove array and a crater-multi-groove array) were obtained on the 7075-T6 aluminium alloy adhesive joints. The effect of pulse energy and groove distance was evaluated over the texture geometry and joint adhesion. Results showed that a two-step laser treatment (pre-crater array and post-multi-groove pattern, respectively) improves the bonding strength of the joint by causing a cohesive failure. These results were attributed to the adoption of the first treatment (crater array) before the groove pattern, which increases the treated area and the Sa roughness parameter. In Ref. [48], to improve mechanical performance and verify adhesive bond degradation due to ageing, a pulsed laser surface pretreatment was applied to aluminium AW 6082-T6 joints with epoxy adhesive E320. This treatment increased single-lap shear (SLS) strengths before and after hydrothermal ageing at 80 °C compared to untreated samples. Results revealed that laser power and pulse frequency were critical for high SLS strengths. Surfaces with significant micro and nanoscale enlargements and deep solidification structures achieved SLS strengths up to 50 MPa and exhibited minimal ageing losses of 4 %. Moroni et al. have studied the influence of laser treatments on the adhesive strength of aluminium alloy in both static [49–51] and cyclic loads [52]. In Ref. [49], the possibility of increasing the mode I strain energy release through the adoption of laser treatments was successfully investigated. In Ref. [50], based on the energy consideration, a predictive model was developed to estimate the texture geometry (the groove's shape and the surface roughness: Sa) by the same authors. However, since the joint strength also depends on the porosity formed at the adhesive-adherent interface and on the mechanical interlocking due to the surface asperities, it is complex to model the strength considering only the surface topography. Then, the response surface methodology was adopted to find the optimal process conditions. In Ref. [51], the authors study the effects of orientations and laser process parameters on the mode I strain energy release rate of Aluminium alloy bonded joints adopting a double cantilever beam (DCB) joint configuration. It was found that the strain energy is mainly affected by the presence of air bubbles entrapped in the surface asperities, which depends on the surface skewness (Ssk). Moreover, the joint's fracture energy is mainly related to the average power, hatch distance, and scanning speed, rather than the orientation, since the latter determines the microstructure geometry. In addition, they found that laser treatments can significantly increase the fatigue life compared to the grit blasting treatment [52].

Although all these studies have consistently shown the possibility of improving adhesion strength and shifting failure modes from adhesive to cohesive, some points remain unresolved, among these: the possibility of regulating the groove's width regardless of the depth, and the possibility of producing treatments that involve both chemical adhesion and effective mechanical anchoring, avoiding, at the same time, microporosity at the interface. To solve this issue, some authors have proposed

the use of multi-step treatments. For instance, in Ref. [53] a chemical treatment was adopted after laser texturing to tune the wettability, achieving superhydrophilicity, superoleophobicity, superhydrophilicity, superoleophobicity, and coexistence of superoleophobicity and superhydrophilicity. In Ref. [29], laser texturing followed by chemical etching was successfully applied as pre-treatment for the brazing operation. Results showed an effective improvement in adhesion. However, the use of multiple treatments, although it leads to an improvement in the joint's strength, results in considerable efforts in terms of time, process complexity, environmental impact, and operators' safety, as well as the loss of the typical advantages of laser processing. Recently, researchers have proposed the adoption of a two-step full laser treatment to modify surface properties [54–56]. Furlan et al. [54] adopt an ns-pulse laser for the Mg alloy AZ31 surface structuring by adopting a two-step laser treatment, consisting of remelting and texturing (by dimpling). To improve the adhesion of carbon fibre reinforced plastic (CFRP), Xie et al. [55] proposed a two-step laser treatment. The first step removes the resin from the outer surface, while the second step produces a texturing (parallel or grid grooves) on the exposed layer. Compared with smooth laminates, double treatment results in a 40.8 % enhancement in the apparent shear strength. In Ref. [56], the researchers investigated the impact of laser surface treatments on the adhesion strength in hybrid structures made of dissimilar materials: AA7075 aluminium alloy and polyether-ether-ketone (PEEK), through friction-assisted joining. A two-stage laser treatment was applied: initially, laser texturing was performed to create a deep square grid, followed by low-energy laser cleaning on the overall surface involved in the adhesion. The results demonstrated that laser cleaning after texturing significantly improved adhesion regardless of the grid size used, demonstrating the potential of the double treatment to enhance the joining of dissimilar materials in hybrid structures. Two-step full laser treatments represent an excellent compromise for industrial needs in terms of process time, costs, adopted equipment, etc. At the same time, they allow taking the full advantage of laser processing. However, the relevant bibliography appears lacking concerning these treatments. Consequently, since the novelty, deep investigations are required to develop more efficient treatments.

In the present work, a two-step process was developed and tested, adopting a 30W pulsed Yb:YAG nanosecond laser source to improve the adhesion between aluminium joints. The process consists of a first phase, laser texturing, where a deep texture is obtained on the aluminium adherents by adopting high pulse energy and many repetitions, followed by a further laser treatment, the laser cleaning, carried out with lower energy content, and applied over the overall adhesion surface, as suggested in Refs. [7,51,56]. Then, the paper addresses two issues, in the first part, the effects of technological parameters on the groove geometry (depth, width, burr height, and taper angle) was investigated, and the possibility to tailoring the groove geometry in terms of dept and width was assessed. The results were adopted for the selection of the texturing conditions. In the second part, a Central Composite Design (CCD) experimental plan was developed and applied to verify the joint adhesion. Single-lap joints were produced by adopting an epoxy system adhesive and different texture geometries. The textures were made of parallel grooves characterised by different depths, widths, and areal densities. Furthermore, samples with only laser cleaning, sandpaper treatment, and acetone cleaning were fabricated too and adopted as references. Apparent shear stress, failure energy, and failure mode were recorded. In both parts, ANalysis Of VAriance (ANOVA) was adopted to assess the statistical significance of the process parameters, while the main effect plot, the interaction plots were used to explain the sample behaviours. Results show that compared to the only textured reference samples, the two-step laser treatment increases the apparent shear stress and the failure energy, regardless of the adopted texture geometry. Then, the laser cleaning post-treatment significantly improves the joint strength.

2. Materials, equipment, and experimental procedures

2.1. Materials

For joint production, the aluminium alloy 6000 series (AA6070 T06) was adopted to produce single-lap joints, according to the ASTM D1002-10 Standards [57]. AA6070 T06 is a precipitation-hardening aluminium alloy containing magnesium and silicon as its major alloying elements. This alloy combines medium strength, good workability, and high corrosion resistance. In plate form, it is the alloy most commonly used for machining. The large amount of manganese allows for control of the grain structure, resulting in a stronger alloy. The higher strength of Aluminium alloy 6082 has seen it replace 6061 in many applications, such as aircraft components, camera lens mounts, marine and scuba components, electrical fittings and connectors, hardware, hinge pins, magneto parts, brake and hydraulic pistons.

Samples of 25 mm × 70 mm in-plane dimension and 3 mm in thickness were obtained by shearing, cleaned in an ultrasonic bath with acetone, and then laser treated according to the procedures reported in the next Paragraphs. Immediately after the laser treatment, the samples were stored in a vacuum bag for a week to avoid surface contamination. Then, single-lap joints were produced by bonding two adherents with the epoxy adhesive Araldite 420 A/B. This is a two-component, room-temperature curing paste adhesive suitable for a range of materials, such as metal, honeycomb, polymers, and fibre-reinforced composites. The main properties of the adhesive are high strength and toughness, high shear strength, good peel strength, low viscosity (35–45 Pas), and a pot life of more than 1 h. During the manufacturing process, a special tool with seven moulds, produced by Fused Deposition Modelling (FDM), was used to maintain the alignment of the adherents, ensure the correct positioning, and avoid possible movements of the components. The adhesive thickness was controlled by applying a weight on the samples (an iron plate of about 2 kg on each tool) during the adhesive cure. After the curing, the adhesive thickness was measured by optical microscopy, resulting in 282 ± 39 μm. Fig. 1 shows the geometry of the adopted single-lap joint. Fig. 2 showss the adherents arranged in the tool before and after the bonding operation. After the demoulding, the samples were post-cured at 60 °C for 6 h. In Table 1, the mechanical and physical properties of adopted materials are reported together with the typical chemical composition of the AA6082 T6 [58].

2.2. Experimental procedures

Since the main aim of the work is to verify the effect of groove geometry and density and the effectiveness of the laser texturing combined with a laser cleaning treatment, two experimental plans were carried out according to the Design of Experiment procedures. First, preliminary tests were carried out to identify the effect of the control factors (i.e. the process parameters) on the groove geometries, adopting a 4 × 5 full factorial experimental plan. Then, a 2 × (2^3+1) Central Composite Designs (CCD) experimental plan was developed and performed by changing the treatment (laser texturing or laser texturing followed by laser cleaning), groove's width and depth, and the areal density, which represents the percentage of texturized area. CCD consists of a fractional factorial design with center point/points and additional axial point/points (not adopted here) that allow estimating first- and second-order terms (i.e. main effects and 2-order interactions) without a significant loss in efficiency. Central composite designs are beneficial in sequential experiments since it is possible to increase the fitting by adding further axial points. It may be adopted in a response variable modelling with curvature since, in a regression model, it allows the estimation of quadratic terms. In addition, compared to the standard fractional factorial multilevel design, it requires fewer experimental runs.

For the preliminary tests, to change the groove's geometry, it was decided to assume the number of parallel lines (L) and the number of repetitions (R) as control factors, where L is how many parallel lines

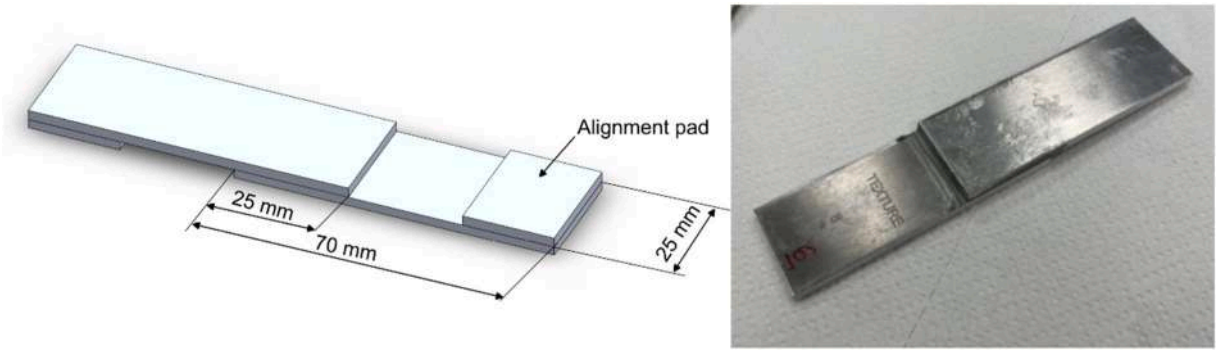

Fig. 1. Geometry and images of the single-lap joint.

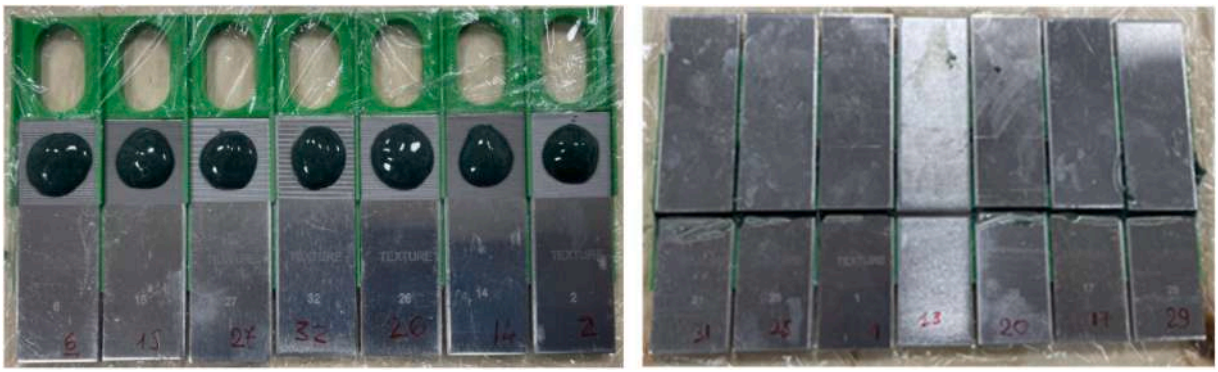

Fig. 2. Images of the AA6082 adherents arranged in the special tool: a) After the adhesive applications; b) After joining.

Table 1
Mechanical, physical properties, and chemical composition of adopted materials.

Property	Units	Al6082 T06 [58]	Araldite 420 A/B
Tensile strength	MPa	290–310	29
Tensile Yield	MPa	250–260	–
Tensile modulus	GPa	69–70	1.49
Elongation at break	%	10	4.6
Density	kg/m^3	27′000	11′000
Thermal conductivity	Wm^{-1}K^{-1}	170–180	n.a.
Specific heat	Jkg^{-1}K^{-1}	0.891	n.a.
Melting point (solidus, liquidus)	°C	556–649	–
Shear strength (LSS)	MPa	205	37
Lap shear strengths	MPa	–	24–35[a]
Gel time	h	–	1
Viscosity (at 20 °C)	mPas	–	35–45

Element for AA6082	Weight %	Element for AA6082	Weight %
Aluminium (Al)	95.2–98.3	Manganese (Mg)	0.40–1.0
Chromium (Cr)	<= 0.25	Silicon (Si)	0.70–1.3
Copper (Cu	<= 0.10	Titanium (Ti)	<= 0.10
Iron (Fe)	<= 0.50	Zinc (Zn)	<= 0.20
Magnesium (Mg)	0.60–1.2	Other, each (Total)	<= 0.05 (<=0.15)

[a] As declared by the Producer, LSS may depend on the materials, thickness and joint characteristics.

were adopted to produce the groove, while R is how many times the laser scanning is performed on the same part of the surface. This assumption was made considering that the former controls the groove width, while the latter controls the depth. Then, a 4x5 full factorial plan was developed and tested, changing according to Table 3. During the tests, the distance between the adjacent lines, the laser power, the pulse frequency, and the scanning speed were fixed at 40 μm, 30 W, 30 kHz, and 1000 mm/s, respectively. These values were selected based on previous studies [56,59–61] since they allow a well-formed open groove with a moderate burr in a reasonable time for the present study.

2.3. Laser equipment

Both the surface treatments were obtained by adopting a MOPA and Q-switched Yb:YAG fiber laser source (IPG, mod. YLP-RA 30-1-50-20-20), working at a wavelength of λ = 1064 nm. The laser beam is moved through a two-axis Galvo scan head (from LASIT) equipped with a "flat field lens", 160 mm of focal length, resulting in a beam spot diameter of about 80 μm. The laser system characteristics are summarised in Table 2. This kind of laser was selected for the good absorption on all metals, high pulse power and pulse energy (up to 20 kW and 1 mJ, respectively), the possibility to deliver the maximum power (30W) at all the frequencies and the lower power consumption (160W, comprises the embedded PC). The latter is critical when considering process sustainability [62–64]. Table 2 shows the main characteristics of the laser

Table 2
Laser systems characteristics.

Characteristic	Symbol	Unit	Value
Source	–		Yb:YAG
Wavelength	λ	nm	1064
Nominal average power	Pa	W	30
Mode		kHz	PW
Pulse frequency	f	kHz	30 ÷ 80
Pulse length	Pl	ns	50
Maximum pulse power	Pp	kW	20[a]
Maximum pulse energy	Pe	mJ	1[a]
Maximum scan speed	Ss	mm/s	5000
Beam quality (M^2)	–	–	1.2 ÷ 1.5
Focused spot diameter	–	μm	80

[a] At Pm = 30 W and F = 30 kHz.

Table 3
Experimental plane for texturing tests (First experimental plan).

		Level				
Control factors	**Label**	−2	−1	0	1	2
Lines	L	2	4	–	6	8
Repetitions	R	20	40	60	80	100

system.

To characterise the groove geometry, the groove's Depth, Width-out, Width-in, Burr eight (Burr), and the Taper angle (Ta), measured as reported in Fig. 3, were adopted as response variables. The measures were analysed by performing the ANalysis Of VAriance (ANOVA). The ANOVA tests the significant differences between the means of the response variables by dividing its total variation into the contribution due to different sources (error, experimental group membership …) and comparing the variance due to the between-groups (or treatments) variability with the one due to the within-group (i.e. the same treatment). A confidence level of 95 % ($\alpha = 0.05$) is adopted during the analysis. Then, a control factor or an interaction is considered statistically significant if the *p*-value is less than 0.05. The ANOVA assumes that experiments are independent and normally distributed with equal variances between cutting conditions. Then, before the analysis, these assumptions were checked by the residuals analysis, as suggested in Refs. [65,66]. However, this analysis is not reported here for the sake of brevity. In addition, the main effect plots and the interaction plot were adopted to determine the effect of the significant control factor on the response variables.

Before joining tests, a two-step laser treatment (LTC) was developed and adopted for the surface treatments. The treatment consists of a first phase, namely laser texturing (LT), where a texture is obtained on the adherents by adopting high energy density (i.e. narrow overlapping along the beam travel and high pulse energy), followed by a further laser treatment, called laser cleaning (LC), carried out at low overlapping and pulse energy, and applied over the overall adhesion surface. All the treatments were obtained by moving the laser beam on the $25 \times 25\ mm^2$ portion of the aluminium sample surface addressed for the bonding, according to the schematic in Fig. 4.

For the laser texturing phase, to highlight the role of the laser cleaning step, a simple linear texture (i.e. grooves placed at 90° respect to the load direction) was adopted, changing the width and the depth of the grooves, in addition, the ratio between the textured and un-textured areas were changed too. All the textures were obtained by fixing the hatch distance (Hd, see also Fig. 4.), scan speed (Ss), and pulse frequency (f) at the same values adopted for the texturing tests and changing the number of parallel lines (L = 2, 4, 6) the number of repetition (R = 20, 40, 60) and the Textured area density (O = 20 %, 35 %, 50 %) that is the

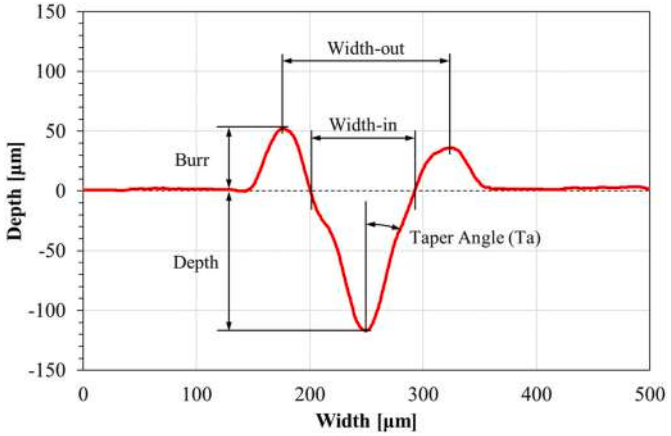

Fig. 3. Schematic of the groove section and the geometrical characteristics.

percentage of textured area. The latter was changed by changing the distance between the grooves (D).

The laser cleaning process was carried out adopting a scan speed of 3000 mm/s, Pa = 24W, Pe = 0.4 mJ, f = 60 kHz, Hd = 50 µm, with a single repetition (R = 1), see Fig. 4. Although laser cleaning is often considered a non-invasive process for the substrate, the adopted process results in a quasi-smooth surface, filled by dimples, 100 µm in diameter, arranged in quincunxes configuration, with minimum overlap and depth (about 3 µm), as visible in Fig. 5, and like some surface treatments studied by Moroni et al. in Refs. [49,67]. The process conditions were selected based on previous experience [7,56], also considering that excessive roughness can easily result in microporosity at the interface that may reduce the joint's strength [50,51]. In addition, samples treated with only laser cleaning (LC), 120 mesh (125 µm) sandpaper (SP) according to the procedure indicated by the adhesive producer [68] and samples without any treatments but cleaned in an ultrasound bath with acetone (as-built samples or AB), have been realised and tested too. Table 4 reports the process conditions adopted for the CCD experimental plan. For each process condition, no less than three samples were realised and tested.

To discriminate the treatment effect (i.e. the joint resistance), tensile tests were carried out according to a modified ASTM D1002-10 Standard [57], at a displacement ratio of 1.27 mm/min, adopting a universal testing machine (MTS INSIGHT 5) equipped with a 50 kN load cell. Then, the apparent shear strength was calculated as the ratio between the maximum load and the joint overlapped area according to the ASTM Standards. Moreover, the energy absorbed up to the failure (Failure Energy or FE) was calculated as the area under the load/displacement curve, as reported in Fig. 6. Digital microscopy (HIROX KH 8700) was adopted to observe and measure the texture geometries and classify, after the tensile test, the failure mode according to the ASTM D1002-10 Standards [57]. After testing, images of the joints were acquired, and the percentage of the adhesive failure mode [AF] was measured through digital image processing (ImageJ and MatLab software). To this end, the images of the failure surfaces were first contrasted and then binarised into black and white. The FA was, therefore, calculated as the sum of the aluminium surface percentage on the two parts of the sample. The results of the tensile tests were analysed through the ANOVA and the main effect and interaction plots.

Moreover, additional tests were conducted on selected samples to explain the adhesion mechanisms. More in detail, Ra roughness parameter was measured for the as-built (AB), Sandpaper (SP) and laser-cleaned (LC) samples, according to the UNI EN ISO 4288:2000, by adopting a portable roughness meter (Taylor Hobson, Surftronic 3^+), the measures were repeated three times on five different samples. Chemical analyses were performed on some AB, SP, LC, LT and LTX samples at various points. The measurements were carried out adopting a scanning electron microscope (SNE ALPHA, SEC Co. Ltd) equipped with an energy dispersive X-ray spectroscopy (EDS) sensor (Oxford Instruments model Xplore compact EDS detector). Wettability tests were conducted using the contact angle measurement method (ASTM: D7334D7334 – 08/2022). The apparent contact angle (θ) was measured through a Tensiometer FTA1000 (First Ten Angstroms, Inc.) according to the procedure reported in Ref. [69]. During the test, a 9,9 ± 0,1 µL drop of glycerol (100 %) was adopted as a reagent since, compared to water, it shows a chemical polarity similar to the epoxy resins [70]. No less than three measurements were performed.

3. Results

3.1. Laser texture and laser cleaning characterisation

In Table 5, the ANOVA results for the groove characteristics are reported in terms of F-value and *p*-value. In the table, the R-Sq and the R-sq (adj) index are reported too, where the R-sq is the amount of variation in the response variable values that is explained by the control factors; R-sq

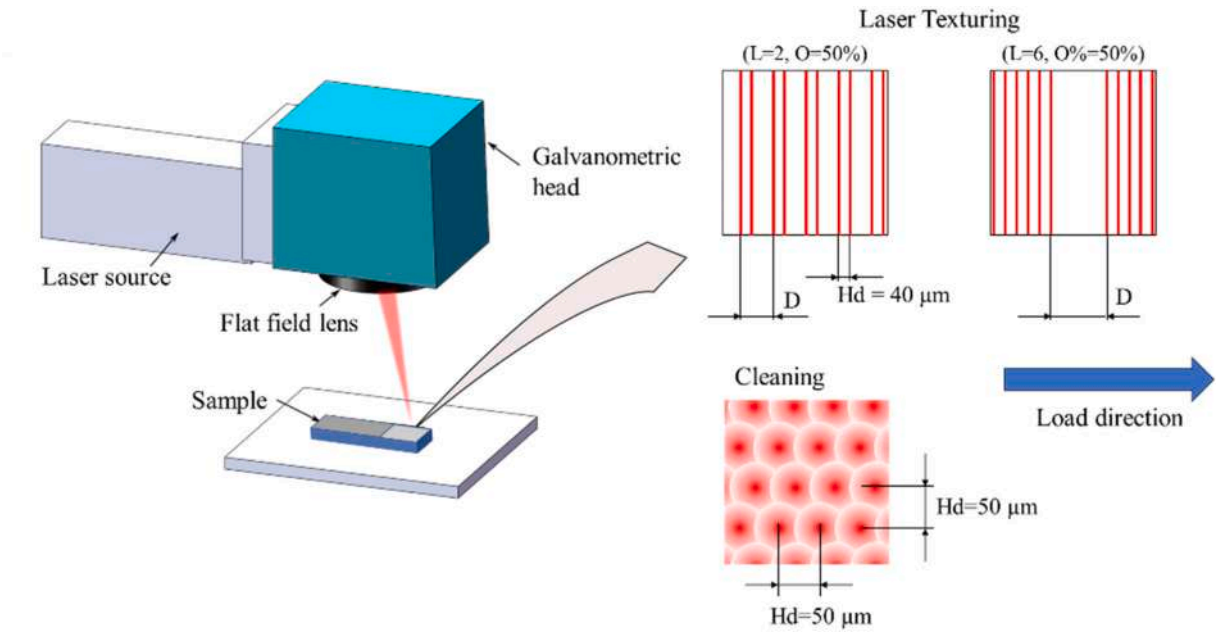

Fig. 4. Schematic of the surface treatments.

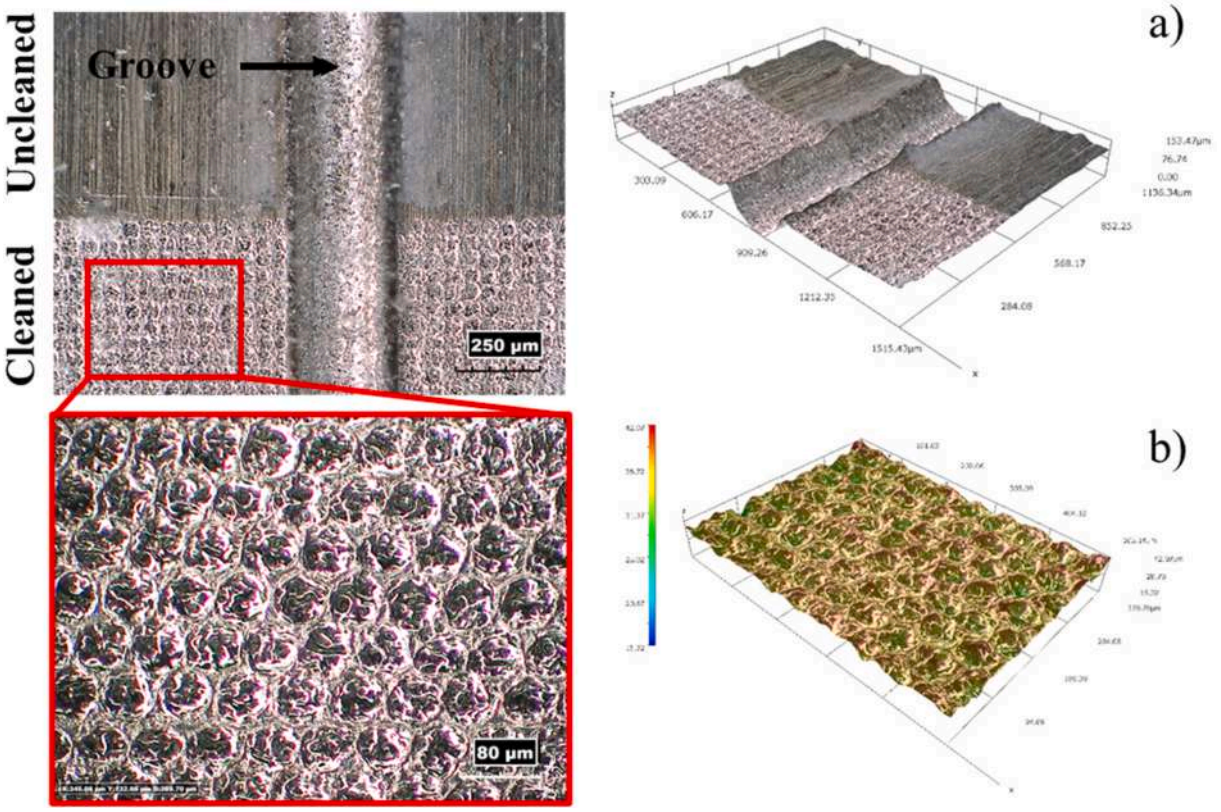

Fig. 5. Images of treated surface: a) Aspect of uncleaned and cleaned surface close to a single groove; b) Magnification of a laser-cleaned surface.

(adj) is a modified R-sq that has been adjusted for the number of terms in the analysis. It is worth noting that the high values of the indexes indicate a good agreement between the statistical model and the data.

From the table, both the control factors affect all the response variables. Moreover, the interaction L*R is significant for the Depth, the Width-out, the Burr and the Taper angle. This means that the effect of one control factor changes as the level of the other changes. It is worth noting that although the p-values of control factors and interaction are less than 0.05, the F-values have different orders of magnitude. In detail, for the Depth, the F-value of R is approximately two orders of magnitude larger than the ones concerning the L and the L*R interaction (557 compared to 7 and 4 for R, L and the L*R, respectively). This means that, compared to the variation of L, a change of R involves a greater Depth variation. The opposite happens for the width, where the F-value

Table 4
Experimental plane for single-lap joint production (in the brackets, the average value of the Width-out and Depth is reported).

Control factors	Label	Level		
		–	0	+
Lines (Width-out µm)[b]	L	2 (142.52 ±5.89)	4 (226.87 ±7.06)[a]	6 (305.63 ±5.98)
Repetition (Depth µm)[b]	R	20 (55.69 ±5.94)	40 (84.16 ±5.56)[a]	60 (108.50 ±6.42)
Textured area percentage	O%	20	35[a]	50
Surface treatment	Tr	LT	–	LT + LC=LTC

[a] Texturing conditions for the central points.
[b] Average and standard deviation values.

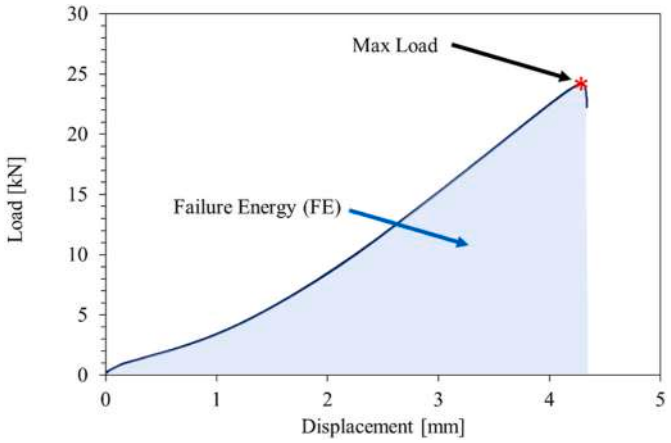

Fig. 6. Schematic of measured quantities from the single-lap joint test.

concerning L is 7495 against the 9 and 2 for the R and the interaction L*R, respectively. In simple terms, the Depth can be easily adjusted by varying R, while the width is adjusted by L.

In Figs. 7–11, the main effect and the interaction plots are reported for the Depth, Width-out, Width-in, Burr and Taper Angle, respectively. From Fig. 7a, as expected, since an increase in the Repetitions involves an increase in the total energy released for unit length, the Depth increases with the R increase. The increment appears linear up to 60 repetitions; after this, a decrease in the slope is observed, and the effect of the number of lines appears more difficult to see since the scale of the diagram is very large compared to the variation of the values. However, this can be deduced from the interaction diagram. From Fig. 7b, it is observed that by increasing the number of L, there is first an increase in depth (between L = 2 and 4) and then a reduction (for R = 40) or the reaching of a plateau (for R > 40). From Figs. 8a and 9a, both the widths linearly increase with L increase. The behaviour with R is very similar; both widths increase as L increases. Regarding the interactions L*R for the Width-out parameter, Fig. 8b, the interaction essentially consists of the fact that for L = 2, the width does not change when R varies. The Burr decreases at L increase and increases at R increase, Fig. 10a. The opposite happens for the Taper angle (Ta), Fig. 11a. Moreover, in both cases, the interaction concerns the behaviour of the curves for the L = 2 condition, which appears different for the other cases (L = 4, 6, 8), Figs. 10b and 11b.

The trends may be explained by considering the three mechanisms involved in material machining: the melting, the vaporisation, and the mechanical effect. The latter is the molten material pullout due to the vaporisation-induced recoil force (so-called recoil pressure [59,71,72]). For the adopted condition, the power density reaches a value of about 10^8 W/cm^2 (20 kW on a beam spot of about 80 µm in diameter). According to Refs. [71,73], the power density is high enough to trigger the keyhole formation. The material melts and increases its temperature up to vaporisation; the vapour pressure blows the molten material out of the groove towards the surrounding area, resulting in the typical Gaussian-like groove, characterised by the burr presence (the rims at the groove edges), as visible in Fig. 12, where the groove profile evolution for L = 2 and L = 6 is reported. However, the energy released in a single laser pass is too low to form a deep groove due to the low pulse energy (Pe = 1 mJ) and high beam speed (1000 mm/s). Conversely, adopting more repetitions (i.e. high released energy), the continuous action of the

Table 5
Extract from the ANOVA results, F-value and *p*-value for Depth, Width-out, Width-in, Burr, and Taper Angle (Significant control factors are highlighted by bold text).

	Depth		Width-out		Width-in		Burr		Ta	
Source	F-value	*p*-value	F-value	*p*-value	F-value	*p*-value	F-value	*p*-value	F-value	*p*-value
Lines	7.41	**0.000**	7495.06	**0.000**	8603.05	**0.000**	15.19	**0.000**	183.20	**0.000**
R	557.83	**0.000**	9.34	**0.000**	30.48	**0.000**	40.22	**0.000**	85.65	**0.000**
Lines*R	4.30	**0.000**	2.76	**0.008**	1.34	0.234	2.98	**0.005**	6.77	**0.000**
R-sq [%]	98.29		99.82		99.85		85.83		96.05	
R-sq(adj) [%]	97.48		99.74		99.77		79.10		94.18	

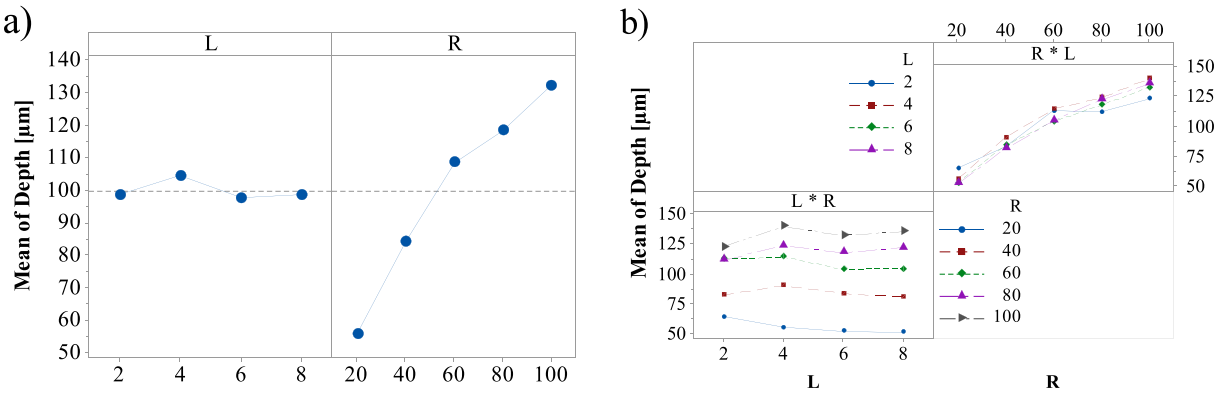

Fig. 7. Depth: a) Main effect plot; b) Interaction plot.

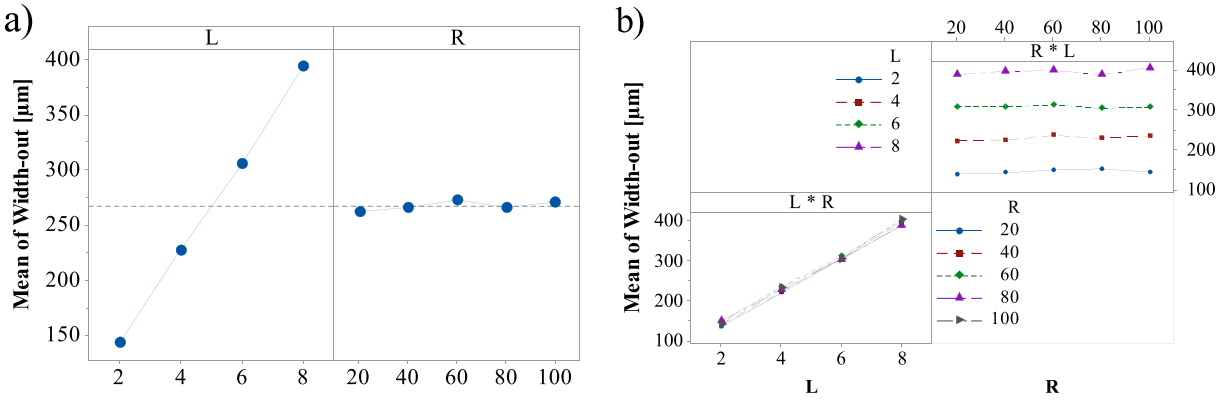

Fig. 8. Width-out: a) Main effect plot; b) Interaction plot.

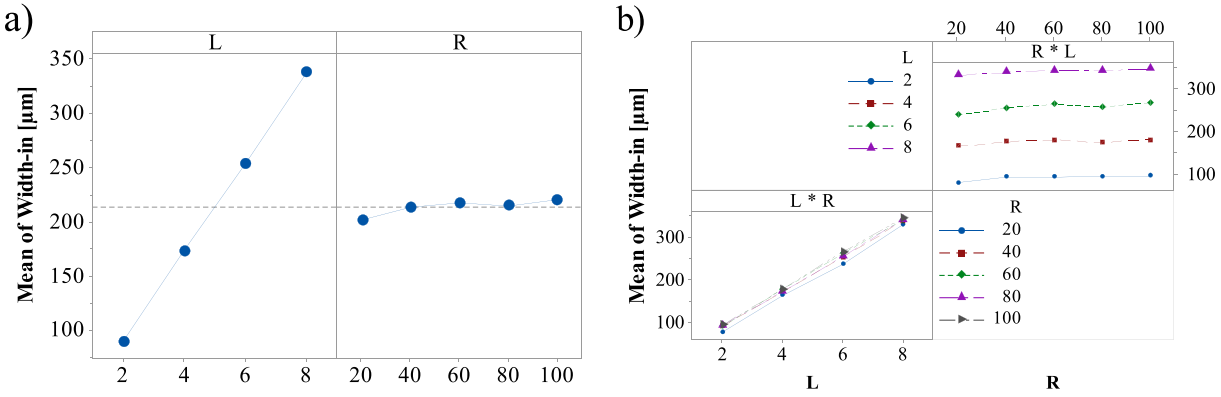

Fig. 9. Width-in: a) Main effect plot; b) Interaction plot.

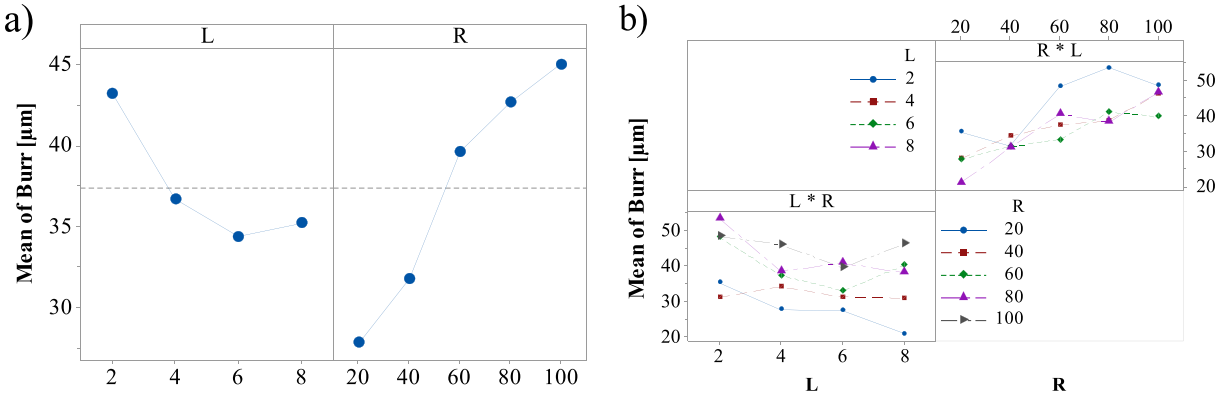

Fig. 10. Burr: a) Main effect plot; b) Interaction plot.

laser beam on the same area increases the groove depth, Fig. 7a, and the burr height, Fig. 10a. Moreover, since the groove width is mainly due to the line numbers, the increase of the depth, due to the R increase, causes a Taper Angle reduction Fig. 11a, this is consistent to Ref. [74].

At the same time, the higher the depth and the lower the width, the greater the difficulty for the vapours to eject the liquid phase. Then, the mechanical effect tends to decrease for narrow grooves (L = 2) and high repetition. Consequently, after a linear increase, a further increase in R results in a slope decrease. Under this condition, the material that is ejected from the groove tends to solidify on the edges, giving rise to an increase and thickening of the burr, as visible in Fig. 12. This explains the behaviour of the depth for L = 2, see Fig. 7b and the effect of R on the Burr, Fig. 11b. Conversely, when large grooves (high L values) are produced, as the depth increases, the molten material that should be ejected from the groove tends to fall inside the groove itself, resulting in a reduction of the burr growth (Fig. 10a), a rounding of the bottom surface (Fig. 12b), and a taper angle reduction (Fig. 11a).

From what is mentioned, it is evident that the material removal process tends to decrease as the depth and width of the groove (i.e. R and L) increase, which is consistent with [59]. Similarly, the increase in the Burr height also tends to reduce. The latter phenomenon is not favourable since the Burr is useful for generating mechanical anchoring phenomena, which improve the adhesive's adhesion. Furthermore, with the same groove density, as R increases, the processing time increases (the latter linearly with R). These aspects are often neglected in the model based on the energy consideration. Moreover, these observations suggest that the number of repetitions and lines adopted during the texture production should not be exceeded. Then, for the texture production, it

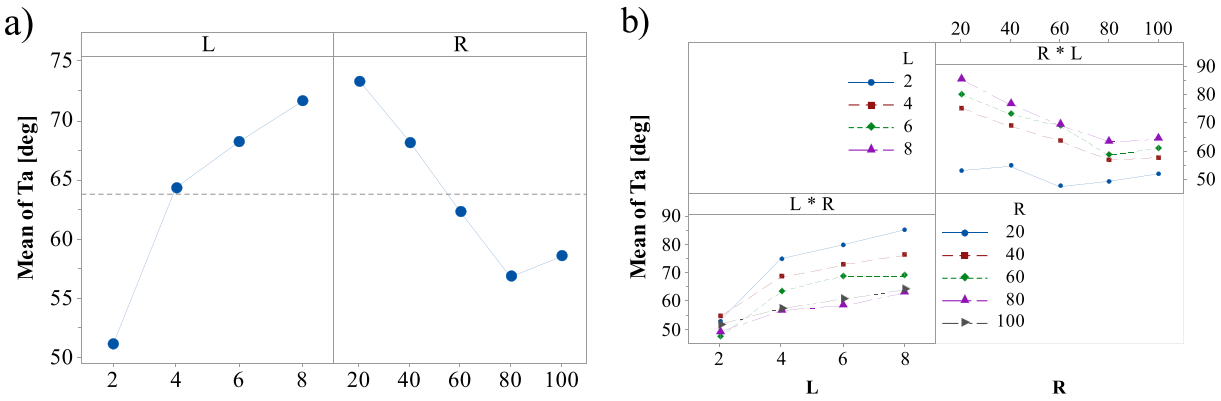

Fig. 11. Taper angle: a) Main effect plot; b) Interaction plot.

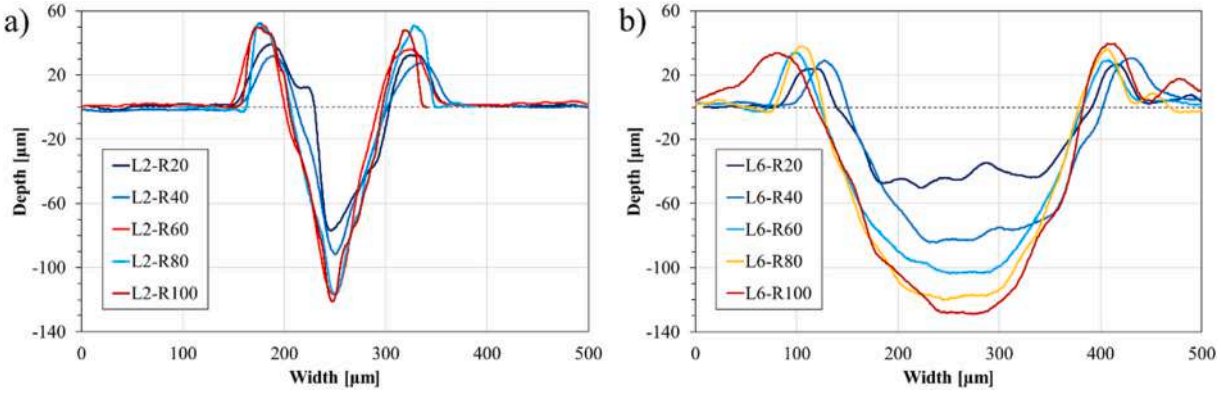

Fig. 12. Groove profiles obtained for different repetitions, for: a) 2 lines; b) six lines.

was decided to fix the maximum number of L and R to 6 and 60, respectively.

3.2. Tensile test results

Fig. 13 shows the different treatments' stress-displacement and absorbed energy-displacement curves. All the curves follow a similar trend regardless of the adopted treatment. The only visible differences are the value of the stress and strain reached during the test and how, once the maximum is exceeded, the curve drops: suddenly for AB and SP samples, slightly slower for laser-treated ones. In Fig. 14, the typical aspects of the failed surface (each image reports the entire bonded surfaces, 25 × 25 mm^2) are reported for the reference (Fig. 14a,b,c), the LT (Fig. 14d,e,f) and the LTC (Fig. 14g,h,i) samples. From the figures, porosity, placed at the adhesive-sample interface or inside the adhesive, is visible irrespective of the surface treatment (as indicated by the black arrows in Fig. 14); the reference samples (AB, SP, and LC treatments) show a percentage of adhesive failure percentage close to 100 % (93 %, 98, and 96 %, respectively). Conversely, the LT and the LTC treatment result in a failure mode that appears like a mixed mode (Fig. 14d,e,g,h) or nearly fully cohesive (Fig. 14f–i).

In Fig. 15, the interval plot for the apparent shear strength is reported for the laser-treated samples (TX and TXC). The dashed lines in the figure represent the average values of AB, SP and laser-cleaned (LC) samples. The LTC treatments show the highest average value, followed by the SP treatment (22.12 ± 1.22), which is one of the treatments suggested by the adhesive producer [68], and then the LT ones. The laser cleaning treatment (LC) results in a value comparable to the SP (21.03

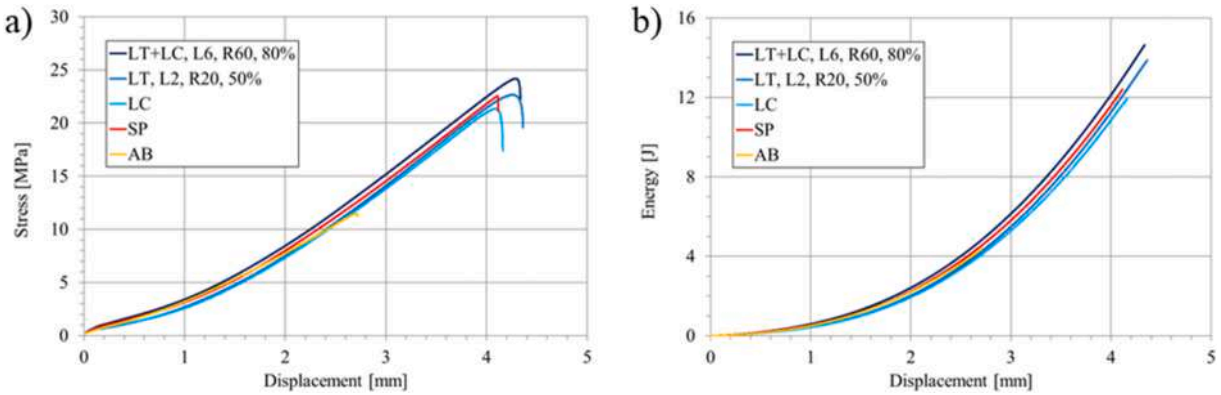

Fig. 13. Single-Lap-Joint tests: a) Stress vs displacement; b) Absorbed energy vs displacement.

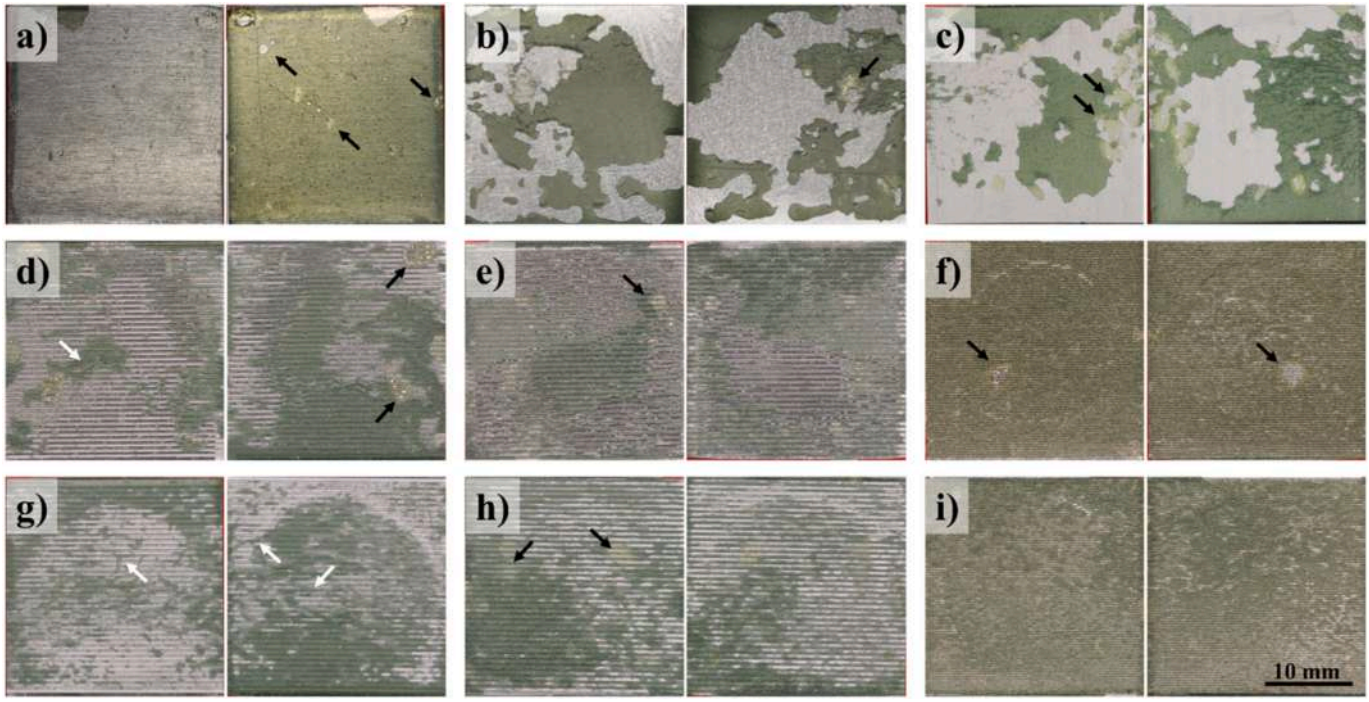

Fig. 14. Images of the entire failure surfaces (25 × 25 mm^2) for samples subject to different treatments. Adhesive failure in a) As-built sample; b) Sandpaper sample; c) Laser-cleaned sample. Mixed mode failure in LT samples: d) L = 6, R = 20, O% = 50; e) L = 4, R = 40, O% = 35; f) L = 2, R = 60, O% = 50; Mixed failure mode in LTC samples: g) L = 6, R = 20; O% = 50; h) L = 4, R = 40, O% = 50; i) L = 2, R = 60, O% = 50.

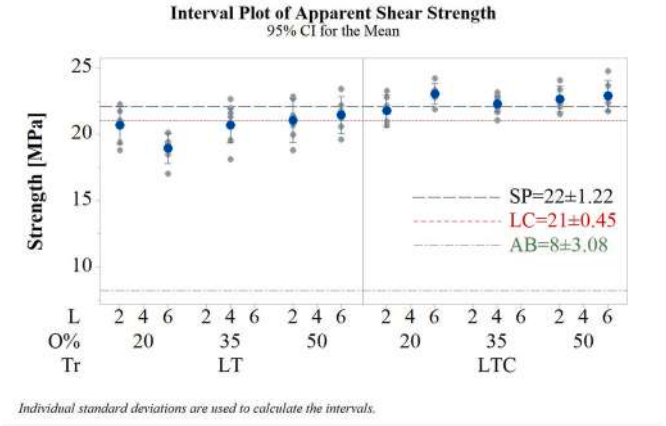

Fig. 15. Interval plot for the Apparent Shear Strength (SP=sandpaper treatment, LC = laser cleaning treatment, AB = as-built).

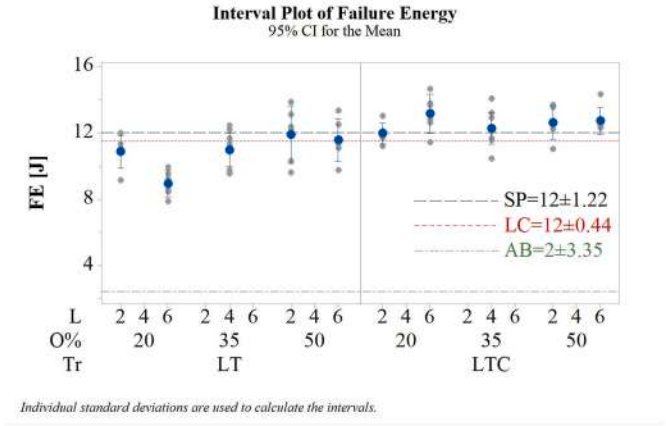

Fig. 16. Interval plot for the Failure Energy (SP=sandpaper treatment, LC = laser cleaning treatment, AB = as-built).

± 0.45) and better than some LT treatments. As expected, the AB samples have the lowest value (8 ± 3.08 MPa), about three times less than the better treatments (SP and LTC).

The interval plot of the Failure Energy, Fig. 16, follows the apparent shear strength trend, with the lowest values for the AB sample and the highest for the SP and LTC treatments.

The behaviour of the adhesive failure percentage (AF) partially follows the strength one, Fig. 17. In fact, for the laser-treated joints, a trend is visible: high resistance corresponds to low AF; for the SP and LC treatments, although their strength is comparable to LT and LTC, AF values close to 97 % and comparable to the AB joints (93 %) were measured. It is worth noting that the failure surface analysis, carried out at high magnifications, revealed the presence of resin filaments protruding from the grooves.

Fig. 18a (in Fig. 14, the filaments are indicated by white arrows), confirming that not all the observable resin is stably attached to the substrate. In addition, several thin and transparent resin islands on the laser-treated joints (LC) can be noted as separate areas (Fig. 18b). Both these events cannot be interpreted by the digital image analysis, introducing underestimation and overestimation of the AF, respectively. Then, the AF, as measured in the present case, does not correctly estimate the actual adhesive failure percentage. However, since the presence of fibrils and resin islands on the surfaces of the laser-treated joints indicates a change in the failure mode for the laser-textured joints (LC, LT, and LTC samples), the AF parameter was maintained in the analysis of the variance, as described in the next paragraph. On the other hand, the proposed DOE contains only the LT and the LTC samples; then, considering that the error is similar for all the laser-treated samples, it may outcome useful information.

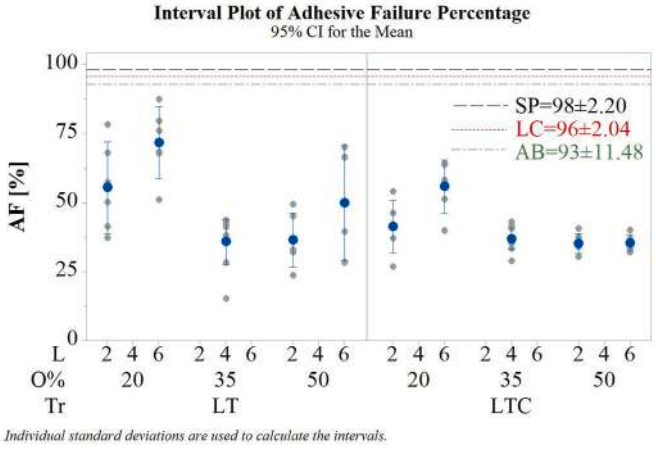

Fig. 17. Interval plot for the adhesive failure percentage (SP=sandpaper treatment, LC = laser cleaning treatment, AB = as-built).

3.3. Effect of process parameters

In Table 6, the ANOVA results in terms of F-value and *p*-value for Apparent Shear Strength (Strength), Failure Energy (FE), and Percentage of Adhesive Failure Mode (AF) are reported. In the table, the significant control factors are highlighted in bold text. From the table, the Textured area density (O%) and the treatment (Tr) affect all the response parameters. Moreover, the failure mode (AF) is affected by the number of lines (L) and the Repetitions (R). The interaction L*Tr is significant for the Strength and FE, while R*O% and O%*Tr are significant only for FE. However, compared to Table 5, the R-sq [%] and R-sq(adj) do not show remarkable values. Probably, it is a consequence of adopting a fractional plan (CCD) instead of a full-factor plan.

In Figs. 19–21, the main effect plots and the interaction plots for the Strength, FE, and AF are reported, respectively. From Fig. 19a, the shear strength increases at the O% increase or when the laser cleaning treatment is applied. The latter has a higher effect than increasing O%, as confirmed by the F-value (41.93 against 6.91 for Tr and O%, respectively). Furthermore, while for the LT joints, the strength decreases as the number of lines increases, for the LTC joints, it increases, as visible in the left panel of the interaction plot, Fig. 19b. This phenomenon, usually referred to as "anti-synergic" effect, tends to hide the influence of R. The same behaviour is observable for Failure Energy (FE), Fig. 20a and b. In addition, FE shows the R*O% and the O%*Tr interactions. The first can be summarised as follows: for R= 20, the energy increases as the number of repetitions increases, the opposite for R = 60 (left panel in Fig. 20c); or, when R = 20, an increase in the textured area leads to an increase in energy, while for R = 60, an increase of O% does not correspond to a change in the energy absorbed up to the failure, which maintains at an intermediate value compared to the extremes ones (right panel Fig. 20c). The second concern the fact that for the LT joints, the Failure Energy increases with the increase of the treated area, while for the LTC ones, it does not change with O% (left panel in Fig. 20d).

Concerning the failure mode, Fig. 21, AF increases with increasing L and decreases with increasing R or O%. At the same time, the laser cleaning post-treatment (LTC samples) has a beneficial effect as it appears to reduce the percentage of adhesive failure area in favour of the cohesive one (Fig. 21a). In contrast, the adhesive failure percentage for the LT joints tends to decrease as the number of repetitions increases, while the LTC ones present a poor sensitivity to this parameter (left panel in Fig. 21b).

3.4. Additional tests

Table 7 shows the roughness measurements performed on the AB, SP, and LC samples. As expected, the SP treatment allows a roughness doubling (from 0.403 ± 0.057 μm to 0.75 ± 0.075 μm for the AB and SP samples, respectively). Also, the laser cleaning allows the Ra parameter to increase, which achieves the value of 0.748 ± 1.185 μm.

Table 8 shows the chemical composition of the AB, SP, LC, LT and LTC treatments. Both the LT and LTC were measured in two different positions: inside the groove and between the grooves on samples obtained adopting L = 6, R = 60, and O% = 20. The chemical analyses do not show significant variations in composition except for the fact that,

Table 6
Extract from the ANOVA, F-value and *p*-value for Apparent Shear Strength (Strength), Failure Energy (FE), and the Adhesive percentage (AF).

	Strength		FE		AF	
Source	F-value	*p*-value	F-value	*p*-value	F-value	*p*-value
L	0.02	0.895	0.71	0.402	19.13	**0.000**
R	0.20	0.661	0.32	0.573	6.66	**0.013**
O%	6.91	**0.011**	11.10	**0.002**	43.95	**0.000**
Tr	41.93	**0.000**	43.54	**0.000**	14.25	**0.000**
L*R	0.84	0.362	3.81	0.056	1.41	0.241
L*O%	0.64	0.428	0.20	0.658	2.86	0.097
L*Tr	4.39	**0.041**	9.20	**0.004**	2.15	0.149
R*O%	3.48	0.068	10.79	**0.002**	0.52	0.473
R*Tr	0.72	0.400	0.38	0.542	26.64	**0.000**
O%*Tr	2.36	0.131	8.79	**0.005**	1.97	0.166
R-sq [%]	54.20		63.12		72.79	
R-sq(adj) [%]	44.51		55.31		67.04	

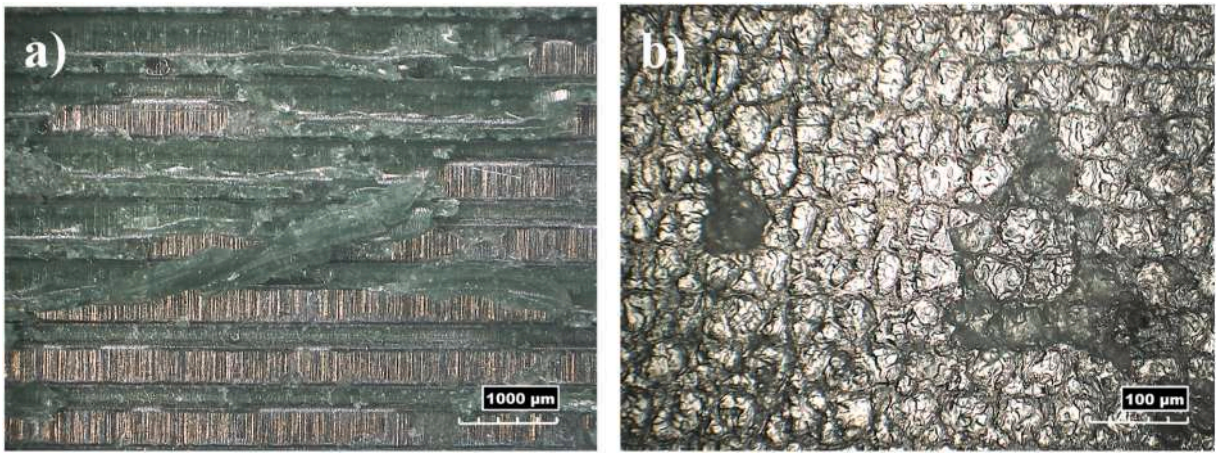

Fig. 18. a) Resin filaments protruding from the grooves; b) Thin resin deposits on the surface of a laser-cleaned sample (LC).

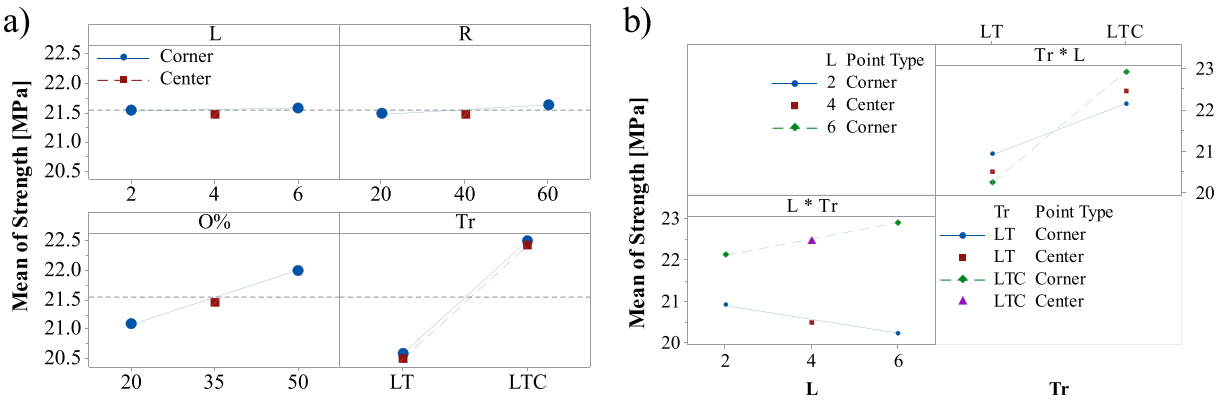

Fig. 19. Apparent shear stress: a) Main effect plot; b) Interaction plot (only significant interaction).

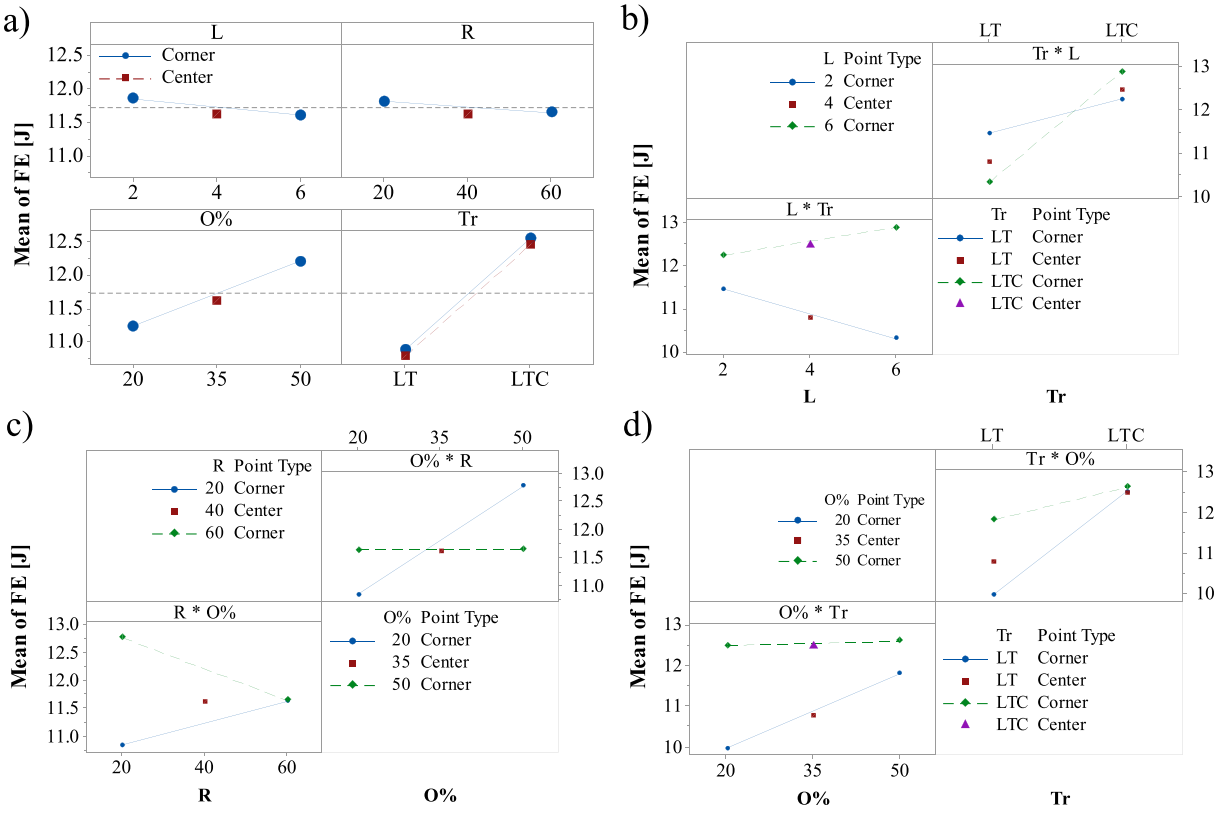

Fig. 20. Failure Energy: a) Main effect plot; b-c-d) Interaction plot (only significant interaction).

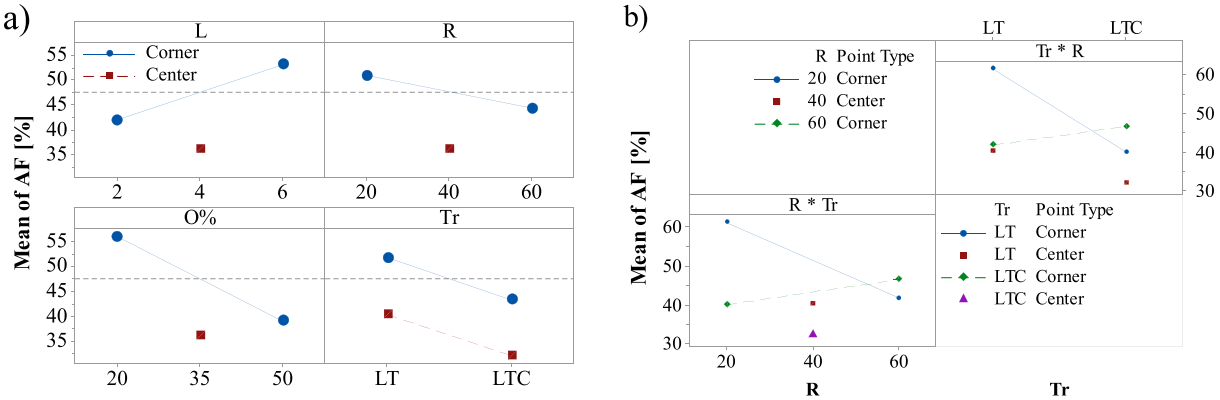

Fig. 21. Adhesive failure mode percentage: a) Main effect plot; b) Interaction plot (only significant interaction).

Table 7
Roughness value for the as-built, Sandpaper and laser-cleaned samples.

Treatment	Average Roughness, Ra [μm]	Standard deviation [μm]
As-built (AB)	0.403	0.057
Sandpaper (SP)	0.748	0.090
Laser cleaning (LC)	1.185	0.075

compared to the as-built, the sandpaper samples show a significant reduction in the Oxygen content (from 6.29 ± 0.47 % to 3.94 ± 0.49 % for the AB and SP samples, respectively). Conversely, all the laser treatments increase the Oxygen content, with a weight percentage measured on the untextured surfaces that is 9.29 ± 0.51 %, 10.02 ± 0.49 %, and 9.46 ± 0.47 % for the LC, LT and LTC, respectively, and about 9.4 % inside the grooves. Furthermore, the Magnesium percentage is higher for the AB samples and between the grooves for the LT treatment (about 1.1 %), lower inside the grooves for the textured samples (0.77–0.78 %), and about 0.9 % for the SP one. Finally, an increase of Manganese content is recorded for the measurement performed inside the grooves for both the LT and LTC samples (about 0.77 % against the 0.45–0.58 % of the other samples). It is important to highlight that analogous surfaces contain comparable chemical species, for example, the composition of the AB surface is like the one placed between two grooves of the LT samples, while the composition of the LC surface is similar to that placed between two grooves of the LTC samples, as well as the surfaces inside the grooves for both LT and LTC. In addition, since the EDS detector cannot discern how the Oxygen is structured (whether it is a metal oxide or is in the form of hydroxide), and at the same time, the presence of aluminium hydroxides on the surface is a common occurrence for untreated aluminium alloys. It is reasonable that although there is a higher oxygen content on the surfaces of laser-treated samples, this is predominantly structured as aluminium oxide instead of aluminium hydroxide. In Fig. 22, a comparison of the chemical composition of the analysed surfaces is reported for all the elements except aluminium.

In Table 9, the average value and the standard deviation of the contact angle (θ) measured between 10 and 60 s after the drop deposition are reported for the AB, SP and LC surfaces. In Fig. 23, the contact angle is reported as a function of the time elapsed since the drop was deposited. From Table 9, since θ decreases, both the treatment SP and LC increase the surface wettability and then the adhesion. Considering only the contact angle, it seems that, compared to the SP treatment, the LC treatment is more effective as it allows lower contact angles. Furthermore, it must be added that the LC treatment does not tend to stabilise since, after 300s, the angle reaches values lower than 4°, values that are difficult to measure.

From the results, compared to the as-built surface, the sandpaper treatment allows the removal of the first surface layer by surface deposits, oxides (about 4 % against 6 % of the AB samples), and compounds due to corrosion or atmosphere reaction, generating a fresh surface that is more reactive with the adhesive (the wettability increases). Consequently, the treatment decreased the activation energy, allowing the formation of chemical bonding or van der Waals interaction forces, as confirmed by the lower contact angle. The sample treated with laser cleaning shows an increase in both roughness and Oxygen percentage (about double compared to the SP), the latter due to the formation of aluminium oxide compound. In any case, both treatments allow a reduction of the contact angle, which passes from 72° for the AB to 58° and 10° for SP and LC treatments, respectively. The contact angle is a function of the chemical species and the surface topography; then, it is plausible that the increase observed for the LC samples is also due to the presence of the micro-texture resulting from this treatment.

4. Discussion

The untreated sample shows the lowest roughness values (Ra = 0.403 ± 0.057) and the highest contact angle values (θ = 72°), in addition, it has a much higher quantity of oxygen (probably both oxide and hydroxide compound) than the treated samples, therefore it can be concluded that, among the analysed surface state (i.e. treatments), it is in the worst conditions to generate both the interlocking mechanisms and the chemical adhesion of the resin. This justifies the observed failure mode (100 % cohesive), the low strength value (8 ± 3.08 MPa), and failure energy (2 ± 3.35 J).

Sandpaper treatment (SP) shows a moderate increase in the roughness (Ra = 0.748 ± 0.900 μm), the lowest oxygen content (3.94 ± 0.49), and a medium wettability (θ = 58°). Thus, compared to the untreated

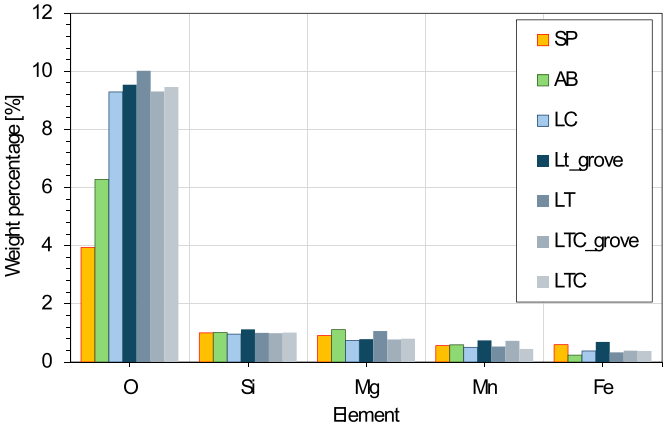

Fig. 22. Chemical composition (only the elements with a weight percentage more than 0.3 %), Al = as remain.

Table 9
Contact angle values (θ) (average value and standard deviation in the period between 10s and 60s).

Treatment	Contact angle [deg]	Standard deviation [deg]
As-built (AB)	72.01	4.37
Sandpaper (SP)	58.24	4.11
Laser cleaning (LC)	10.21	2.34

Table 8
Chemical composition measured through EDX analysis on the sample surfaces.

Treatment	AB	SP	C	LT[a]	LT[b]	LTC[a]	LTC[b]
Component							
Al [%]	90.78 ± 0.48	92.99 ± 0.51	88.13 ± 0.53	87.05 ± 0.51	87.13 ± 0.66	87.90 ± 0.48	87.82 ± 0.51
O [%]	6.29 ± 0.47	3.94 ± 0.49	9.29 ± 0.51	10.02 ± 0.49	9.54 ± 0.62	9.46 ± 0.47	9.31 ± 0.49
Si [%]	1.01 ± 0.14	1.00 ± 0.13	0.96 ± 0.14	1.00 ± 0.13	1.12 ± 0.18	1.01 ± 0.12	0.99 ± 0.13
Mg [%]	1.11 ± 0.08	0.91 ± 0.08	0.74 ± 0.84	1.06 ± 0.08	0.78 ± 010	0.80 ± 0.08	0.77 ± 0.08
Mn [%]	0.58 ± 0.10	0.56 ± 0.12	0.50 ± 0.12	0.53 ± 0.12	0.74 ± 0.14	0.45 ± 0.10	0.72 ± 0.12
Fe	0.24 ± 0.10	0.59 ± 0.13	0.38 ± 0.12	0.33 ± 0.13	0.69 ± 0.16	0.38 ± 0.10	0.37 ± 0.37

[a] Measurement between two grooves.
[b] Measure inside the grooves.

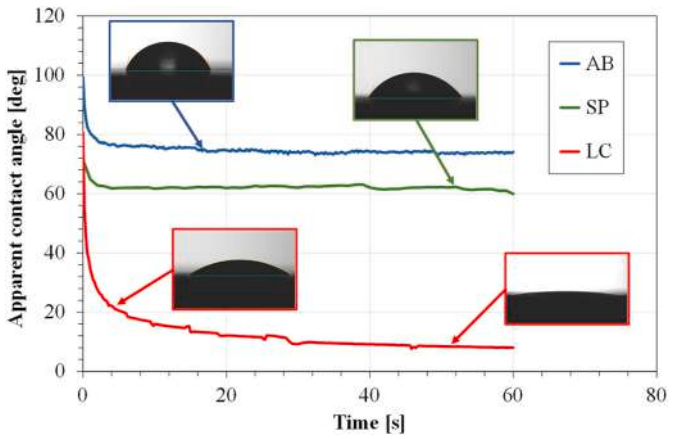

Fig. 23. Dynamic contact angle behaviours on AB, SP and LC samples (sessile drops method, with glycerol).

samples (AB), this treatment shows a better adhesion. Therefore, both the apparent shear strength and failure energy increase by about 2.7 and 6 times, respectively, as visible in Figs. 15 and 16. However, since the increase in roughness is modest, it does not produce effective interlocking mechanisms, and the fracture mode results close to 100 % adhesive failure.

Even laser cleaning alone increases the roughness (Ra = 1.185 + 0.075 μm) and cleans the surface from residues of possible contaminants, generates a micro-texture (see Fig. 5) that allow an increase in resistance and absorbed energy, which is slightly lower than that of the SP treatment (Figs. 15 and 16). In any case, due to the moderate increase of the roughness, the joint failure is almost adhesive, as confirmed by the high value of the AF parameter.

The laser texturing (LT) treatment results in more complex mechanisms since it increases the effective bonding area and promotes mechanical anchoring, as confirmed by the mist mode failure. However, at the same time, the presence of the texture and its burrs increases the local stress and the peeling components [75,76]. This phenomenon is aggravated by the possibility that the grooves on the two faces are arranged opposite each other, as reported in Fig. 24, The latter condition generates a narrow cleft which results in a further increase in the concentration of stresses around the groove, so much so that in more than one case the burr separation from the metallic surface and its embedding into the adhesive was observed (see red arrows in Fig. 25a). In addition, the presence of residues from processing (splashes and condensed metal) may generate an incoherent surface in correspondence with the grooves, which may favour the adhesive debonding. Furthermore, the smooth part enclosed between two burrs (that for the LT samples is an untreated surface) behaves differently depending on the distance between the grooves (the D parameters of Fig. 4): if D is sufficiently small, it acts as a trap for the adhesive with the consequence that the fracture propagates into the adjacent adhesive layer or deviates towards the other face, allowing the strength increase, as visible in Fig. 25a, where a homogeneous layer of fractured adhesive is visible. If it is long, the adhesive is removed from the smooth surface, as visible in Fig. 25b, where the uncleaned surface between the grooves is present. This phenomenon does not change for a high number of passes (R = 60), Fig. 25c and large D, except for the fact that for narrow grooves (L = 2), the adhesive layer is present on most parts of the failure surface Fig. 25c. These observations explain the strong dependence of the strength on the O% since the latter is a function of the D parameter. Furthermore, they suggest that the surfaces between the grooves play a fundamental role in determining joint behaviour and the failure propagation mode. All that accounts for the modest gains in resistance compared to the SP treatment (average strength is comprised in the interval 18–21 MPa, while the failure energy is in the interval 9–12 J) and the reliance on the percentage of the treated area (O% up to 75 %).

Adopting the laser cleaning step after laser texturing further enhances the joint's strength by increasing adhesion on the flat surfaces between the grooves. As a matter of fact, laser cleaning improves the adhesion of the untreated area, joint's strength, and failure energy by forming an oxide layer and micro-texture, which improve the wettability and promote mechanical anchoring at the micro-level, as confirmed by the presence of thin resin islands on the failure surface (see. Fig. 18b). This is also confirmed by the analysis of Figs. 15 and 16, or when the surfaces obtained for the LT are compared with the LTC ones. In Fig. 26, the failure surfaces obtained for the central points (L = 4, R = 40, O% = 35) for the LT and LTC treatments are compared. In the figure, the adhesive layer concerning the LT treatment appears to replicate the opposite surface (the metal one), with the texture produced by the sheet metal rolling process well replicated on the adhesive layer. Conversely, for the LTC treatment, the adhesive surface appears irregular and rich in cracks, which confirms the contribution of the micro-texture to the adhesion, and the tendency to produce fractures inside the adhesive rather than at the interface.

In summary, it can be stated that laser texturing allows the creation of mechanical anchoring and, consequently, fracture deviation. Both phenomena allow for an increase in joint resistance compared to the treated joint (AB sample). Laser cleaning significantly improves the adhesion (as confirmed by the wettability tests and by the resistance of the joints treated only with laser cleaning). Adopting both treatments

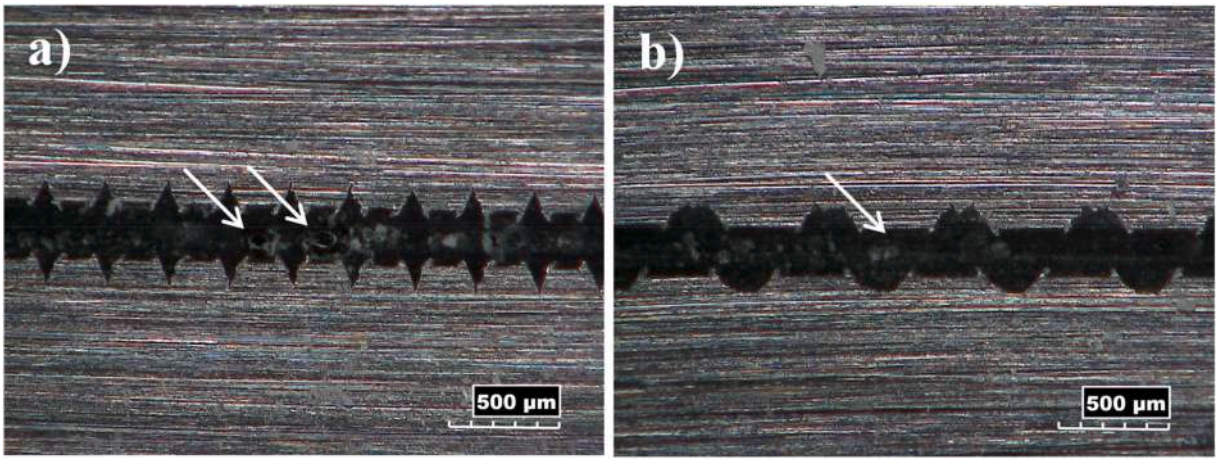

Fig. 24. Possible arrangement of the groves: a) Grooves alignment for a sample treated at L = 2, R = 60, O% = 50; b) Grooves unalignment for a sample treated at L = 6, R = 60, O% = 50 %. In the figures, the arrows indicate the presence of porosity.

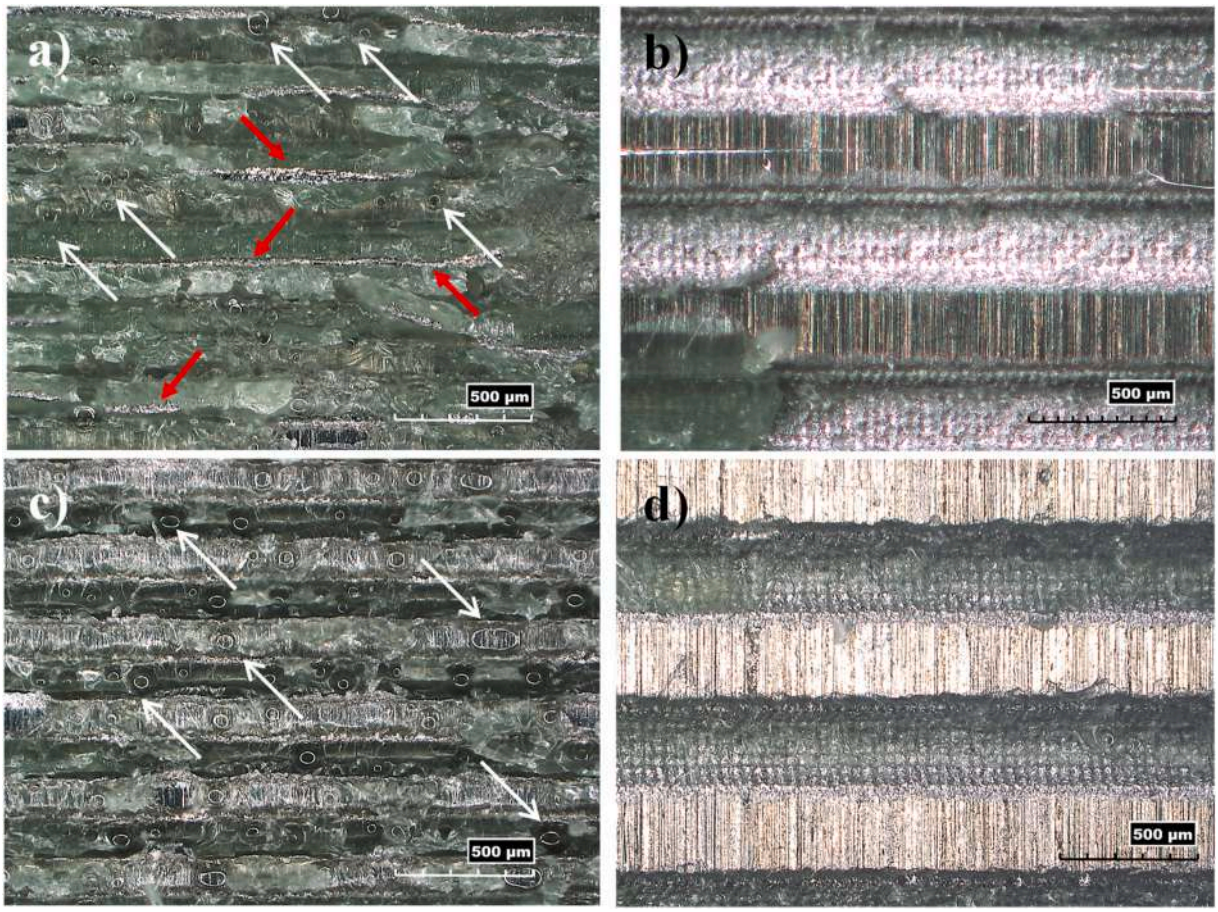

Fig. 25. Appearance of failed surface for LT treatment at: a) L = 2, R = 20, O% = 50; b) L = 6, R = 20, O% = 50; c) L = 2, R = 60, O% = 50; d) L = 6, R = 60, O% = 50. In the figures, the white arrows indicate the presence of porosity, while the red ones indicate the burr failure. (For interpretation of the references to colour in this figure legend, the reader is referred to the Web version of this article.)

results in a synergistic effect that further improves the resistance of the joints beyond the value found with the SP treatment, making it less dependent on the adopted process parameters (L, R, and O%).

It is worth noting that the values found among the best laser treatments (about 23.35 ± 0.71 MPa and 21.03 ± 0.45 MPa for the best LTC and the LC samples, respectively) do not differ significantly from that of the Sandpaper treatment (22.11 ± 1.22 MPa). However, from an industrial application point of view, laser treatments have greater flexibility and potential applications. Being easily automatable, they do not require extensive manual activity; since it is possible to carefully select the treated area, masking and mask removal operations are avoided; they do not require consumables and do not produce significant waste, in addition, on relatively small components the process can be easily confined in the laser system, avoiding unnecessary risks for the workers' health.

Among the treatments, the laser cleaning treatment is the one that best suits industrial needs since even if it results in lower resistance, it is considerably faster (here, whit a 30W laser sources, 50 cm^2/s) than the texturing treatment (which is about two orders of magnitude slower) and does not imply the formation of deep grooves that could, in the long term, compromise the resistance of the base material. Then, considering the availability of nanosecond laser sources with high average power (up to 500W), which may significantly reduce the treatment times, enhancing its industrial viability.

5. Conclusion

A two-step laser surface treatment was developed and applied to increase the adhesion of aluminium-aluminium joints obtained by epoxy-paste adhesive. Preliminary tests were carried out to study the effect of technological process parameters (lines and repetition) on the groove geometry. A central composite design (CCD) was adopted, and single-lap joints were produced and tested by changing the laser treatment (LT or LTC), the number of Lines (L), the number of repetitions (R) and the percentage of treated surface (O%). As references, laser cleaning (LC), Sandpaper treatment (SP), and as-built (AB) samples were adopted. From the results, for the assumed laser source and within the experimental conditions adopted in this work, the main conclusions are the following:

- The width and depth of the single groove can be easily sized by changing the number of Lines and Repetitions adopted during the texturing, respectively. The percentage of textured area can be easily changed by adjusting the distance between one groove and the other (here called D).
- On the contrary, both the burr height and the taper angle present smaller variations but more complex relationships with the process parameters, as they are a consequence of how molten material is ejected out of the groove and, thus, the groove geometry itself.
- Compared to the as-built material, all the treatments significantly increase the Apparent Shear Strength and the Failure Energy.
- The post-mortem analysis shows an adhesive failure percentage close to 100 % for the AB, SP and LC samples. Conversely, for all the laser-textured samples, the high magnification images indicate mixed failure mode, with the laser cleaning process ensuring that a more

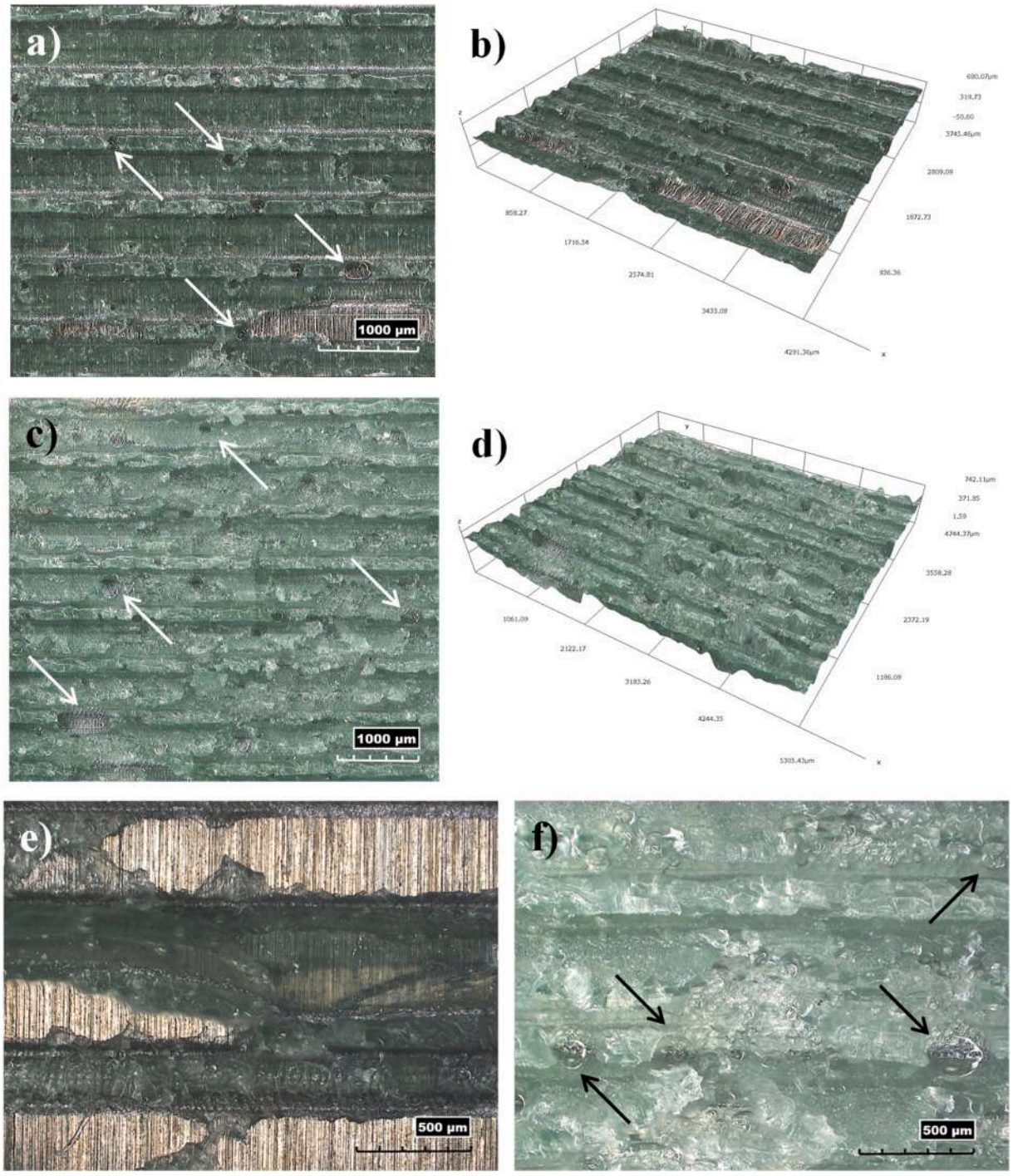

Fig. 26. Appearance of the failed surface at L = 4, R = 40, O% = 35 for a-b) laser-textured sample; c-d) laser-textured and cleaned sample; e) laser-textured sample @ 150 magnification; f) laser-textured and cleaned sample @ 150 magnification. In the figures, the arrows indicate the porosity.

substantial amount of adhesive remained within the grooves of the samples (AF between 35 and 71 %).

- From the ANOVA, the main significant parameters are the adoption of the laser cleaning and the percentage of treated area. While the groove width and the depth have a marginal effect.
- The laser texturing allows the production of the mechanical anchoring and, consequently, the fracture deviation. This results in an increase in the joint strength and the failure energy. The higher the number of grooves and burrs, the higher the failure load.
- The laser cleaning treatment improves the surface adhesion and then the joint's strength; however, due to the moderate roughness increase, it does not permit the formation of effective mechanical anchoring.
- The two-step treatment results in a synergic effect that further improves the resistance of the joints and makes it less dependent on the adopted process parameters.
- Among all the treated samples, those with the highest values of strength before failure are the LTC involving 2 and 6 overlapped grooves and 50 % of the treated area (about 23 MPa). These treatments show a strength that is approximately 3 times higher than the AB samples and slightly higher than the SP treatment.

- Since the laser cleaning post-treatment improves the failure stress irrespective of the other process parameters, the adoption of a large distance between the grooves (low O%) may result in lower process time.
- Furthermore, since the only laser cleaning treatment results in a very short process time and a strength that differs less than 10 % from the best treatment, it may be a favourable process in several industrial fields.

CRediT authorship contribution statement

Davide Morello: Writing – original draft, Investigation, Formal analysis, Data curation, Writing – review & editing. **Claudio Leone:** Writing – original draft, Resources, Methodology, Formal analysis, Data curation, Conceptualization, Writing – review & editing. **Giuseppe Lamanna:** Writing – original draft, Investigation, Formal analysis. **Genna Silvio:** Writing – original draft, Resources, Investigation, Formal analysis, Conceptualization, Writing – review & editing.

Declaration of competing interest

Claudio Leone reports equipment, drugs, or supplies was provided by CIRTIBS Research Centre, University of Campania Luigi Vanvitelli, Via Roma 29, 81031 Aversa (CE), Italy. If there are other authors, they declare that they have no known competing financial interests or personal relationships that could have appeared to influence the work reported in this paper.

Acknowledgement

The authors are particularly grateful to the Interuniversity Research Centre CIRTIBS of the University of Campania Luigi Vanvitelli for providing part of the equipment to develop this research work.

Data availability

Data will be made available on request.

References

[1] Georgantzia E, Gkantou M, Kamaris GS. Aluminium alloys as structural material: a review of research. Eng Struct 2021;227:111372. https://doi.org/10.1016/j.engstruct.2020.111372.
[2] Sun Y. The use of aluminum alloys in structures: review and outlook. Structures 2023;57:105290. https://doi.org/10.1016/j.istruc.2023.105290.
[3] Kaya İ, Başer TA, Kahraman N. Mechanical properties and corrosion behavior of similar/dissimilar resistance spot welded automotive aluminum alloys. Mater Werkst 2023;54:1433–43. https://doi.org/10.1002/mawe.202200200.
[4] Hirsch J, Al-Samman T. Superior light metals by texture engineering: optimized aluminum and magnesium alloys for automotive applications. Acta Mater 2013;61:818–43. https://doi.org/10.1016/j.actamat.2012.10.044.
[5] Martinsen K, Hu SJ, Carlson BE. Joining of dissimilar materials. CIRP Ann 2015;64:679–99. https://doi.org/10.1016/j.cirp.2015.05.006.
[6] Zhang C, Zhang Y, Chen L, Chen Y. Effect of laser micromachining crater-array–multi-grooves on the bonding strength and failure mode of aluminum alloy adhesive joints. Opt Laser Technol 2024;175:110803. https://doi.org/10.1016/j.optlastec.2024.110803.
[7] Mandolfino C, Lertora E, Genna S, Leone C, Gambaro C. Effect of laser and plasma surface cleaning on mechanical properties of adhesive bonded joints. Proced CIRP 2015;33:458–63. https://doi.org/10.1016/j.procir.2015.06.054.
[8] Skeist I. Handbook of adhesives. 1990. p. 77–90. https://doi.org/10.1016/0016-0032(62)90851-7.
[9] Dillard DA. Advances in structural adhesive bonding. second ed. Woodhead Publishing; 2022.
[10] Tiringer U, Kovač J, Milošev I. Effects of mechanical and chemical pre-treatments on the morphology and composition of surfaces of aluminium alloys 7075-T6 and 2024-T3. Corros Sci 2017;119:46–59. https://doi.org/10.1016/j.corsci.2017.02.018.
[11] Li J, Li Y, Huang M, Xiang Y, Liao Y. Improvement of aluminum lithium alloy adhesion performance based on sandblasting techniques. Int J Adhesion Adhes 2018;84:307–16. https://doi.org/10.1016/j.ijadhadh.2018.04.007.
[12] Salstela J, Suvanto M, Pakkanen TT. Influence of hierarchical micro-micro patterning and chemical modifications on adhesion between aluminum and epoxy. Int J Adhesion Adhes 2016;66:128–37. https://doi.org/10.1016/j.ijadhadh.2015.12.036.
[13] Sinmazçelik T, Avcu E, Bora MÖ, Çoban O. A review: fibre metal laminates, background, bonding types and applied test methods. Mater Des 2011;32:3671–85. https://doi.org/10.1016/j.matdes.2011.03.011.
[14] Molitor P, Barron V, Young T. Surface treatment of titanium for adhesive bonding to polymer composites: a review. Int J Adhesion Adhes 2001;21:129–36. https://doi.org/10.1016/S0143-7496(00)00044-0.
[15] Li H, Xu W, Li L, Xia H, Chen X, Chen B, et al. Enhancing the wettability for 4043 aluminum alloy on 301L stainless steel via chemical-etched surface texturing. J Mater Process Technol 2022;305:117577. https://doi.org/10.1016/j.jmatprotec.2022.117577.
[16] Critchlow GW, Brewis DM. Review of surface pretreatments for aluminium alloys. Int J Adhesion Adhes 1996;16:225–75. https://doi.org/10.1016/S0143-7496(96)00014-0.
[17] Marques AC, Mocanu A, Tomić NZ, Balos S, Stammen E, Lundevall A, et al. Review on adhesives and surface treatments for structural applications: recent developments on sustainability and implementation for metal and composite substrates. Materials 2020;13:5590. https://doi.org/10.3390/ma13245590.
[18] Naat N, Boutar Y, Naïmi S, Mezlini S, Silva LFM Da. Effect of surface texture on the mechanical performance of bonded joints: a review. J Adhes 2023;99:166–258. https://doi.org/10.1080/00218464.2021.2008370.
[19] Zou X, Liu L, Chen T, Wu L, Chen K, Kong L, et al. Laser surface treatment to enhance the adhesive bonding between steel and CFRP: effect of laser spot overlapping and pulse fluence. Opt Laser Technol 2023;159:109002. https://doi.org/10.1016/j.optlastec.2022.109002.
[20] Feng Z, Zhao H, Tan C, Zhu B, Xia F, Wang Q, et al. Effect of laser texturing on the surface characteristics and bonding property of 30CrMnSiA steel adhesive joints. J Manuf Process 2019;47:219–28. https://doi.org/10.1016/j.jmapro.2019.09.046.
[21] Ragusich A, Taillon G, Meunier M, Martinu L, Klemberg-Sapieha JE. Selective pulsed laser stripping of TiAlN erosion-resistant coatings: effect of wavelength and pulse duration. Surf Coating Technol 2013;232:758–66. https://doi.org/10.1016/j.surfcoat.2013.06.092.
[22] Gu J, Su X, Li W, Xin M, Zhang D, Jin Y, et al. Investigation on laser paint stripping of CFRP: morphological evolution, damage mechanism, and adhesive performance. J Mater Res Technol 2024;31:3690–37021. https://doi.org/10.1016/j.jmrt.2024.07.063.
[23] Xu M, Yang S, Liu X, Li L, Wan Y, Wang C, et al. Characterization of a two-step laser paint stripping process on CFRP. Compos Struct 2024;339:118140. https://doi.org/10.1016/j.compstruct.2024.118140.
[24] Zhang HX, Hou Y-C, Li Y-F, Yang Y-F, Li K, Yue J-F, et al. Surface quality study of paint stripping on aircraft skins with high energy nanosecond pulsed laser cleaning. Front Physiol 2025;13:1505581. https://doi.org/10.3389/fphy.2025.1505581.
[25] Hou L, Yin F, Wang S, Sun J, Yin H. A review of thermal effects and substrate damage control in laser cleaning. Opt Laser Technol 2024;174:110613. https://doi.org/10.1016/j.optlastec.2024.110613.
[26] Genna S, Leone C, Mingione E. Surface cleaning of 34CrMo4 steel pipes by using pulsed fibre laser. Int J Adv Manuf Technol 2022. https://doi.org/10.1007/S00170-022-10648-8.
[27] Narayanan V, Singh R, Marla D. Optimization of nanosecond pulsed laser cleaning of rust. Lasers Manuf Mater Process 2025;12:68–85. https://doi.org/10.1007/s40516-025-00282-z.
[28] Mateo MP, Nicolas G, Piñon V, Ramil A, Yañez A. Laser cleaning: an alternative method for removing oil-spill fuel residues. Appl Surf Sci 2005;247:333–9. https://doi.org/10.1016/j.apsusc.2005.01.086.
[29] Li H, Xia H, Li L, Li L, Su X, Peng J, et al. Enhancing the reliability of laser welded-brazed aluminum/stainless steel joints via laser-chemical hybrid surface texturing. Thin-Walled Struct 2024;199:111780. https://doi.org/10.1016/j.tws.2024.111780.
[30] Qiang W, Yingchun G, Baoqiang C, Bojin Q. Laser cleaning of commercial Al alloy surface for tungsten inert gas welding. Baoqiang, C , Bojin. Q J Laser Appl 2016;28:022507. https://doi.org/10.2351/1.4943909.
[31] Coddet C, Montavon G, Ayrault-Costil S, Freneaux O, Rigolet F, Barbezat G, et al. Surface preparation and thermal spray in a single step: the PROTAL process - example of application for an aluminum-base substrate. J Therm Spray Technol 1999;8:235–42. https://doi.org/10.1361/105996399770350467.
[32] Li H, Costil S, Liao HL, Coddet C. Role of the laser surface preparation on the adhesion of Ni-5%Al coatings deposited using the PROTAL process. J Therm Spray Technol 2006;15:191–7. https://doi.org/10.1361/105996306X108011.
[33] Gacs J, Sára Bogya E, Kocsis L, Jacob T. Application of laser cleaning on AlMg4.5Mn0.4 sheets for adhesive bonding. Int J Adhesion Adhes 2022;115:103132. https://doi.org/10.1016/j.ijadhadh.2022.103132.
[34] Shi T, Wang C, Mi G, Yan F. A study of microstructure and mechanical properties of aluminum alloy using laser cleaning. Yan. F J Manuf Process 2019;42:60–6. https://doi.org/10.1016/j.jmapro.2019.04.015.
[35] Zhu G, Xu Z, Jin Y, Chen X, Yang L, Xu J, et al. Mechanism and application of laser cleaning: a review. Opt Laser Eng 2022;157:107130. https://doi.org/10.1016/j.optlaseng.2022.107130.
[36] Wang A, Feng A, Gu X, Pan X, Yu J, Jiang Z. Effect of picosecond laser cleaning on surface morphology and properties of stainless steel. Opt Laser Technol 2023;159:109041. https://doi.org/10.1016/j.optlastec.2022.109041.
[37] Akman E, Bora MÖ, Çoban O, Oztoprak BG. Laser-induced groove optimization for Al/CFRP adhesive joint strength. Int J Adhesion Adhes 2021;107:102830. https://doi.org/10.1016/j.ijadhadh.2021.102830.

[38] Schanz J, Meinhard D, Dostal I, Riegel H, Silva AKM De, Harrison DK, et al. Comprehensive study on the influence of different pretreatment methods and structural adhesives on the shear strength of hybrid CFRP/aluminum joints. J Adhes 2022;98:1772–800. https://doi.org/10.1080/00218464.2021.1938004.
[39] Li H, Zhu Y, Meng X, Li S, Du W, Qin X. Effect of laser generated microgrooves geometric parameters on the shear strength of CFRP-Aluminium alloy adhesive joints. J Adhes 2023;99:1744–67. https://doi.org/10.1080/00218464.2022.2158731.
[40] Parodo G, Polini W, Sorrentino L, Turchetta S. Influence of laser texturing on mechanical performances of CFRP single lap bonded joint. 2023. p. 351–6. https://doi.org/10.1007/978-3-031-28547-9_40.
[41] Liu H, Weibel JA, Sabau AS, Geoghegan P, Chen J, Groll EA. Adhesive bonding of copper prepared by laser-interference near the interference structuring limits. Materials 2021;14:3485. https://doi.org/10.3390/ma14133485.
[42] Maressa P, Anodio L, Bernasconi A, Demir AG, Previtali B. Effect of surface texture on the adhesion performance of laser treated Ti6Al4V alloy. J Adhes 2014;91:518–37. https://doi.org/10.1080/00218464.2014.933809.
[43] Çakir FH. Enhancing the adhesive bonding strength of Ti6Al4V sheets with fiber laser texturing. Int J Adhesion Adhes 2022;114:103117. https://doi.org/10.1016/j.ijadhadh.2022.103117.
[44] Zdravković N, Klobčar D, Milčić D, Zupančič M, Žužek B, Milčić M, et al. Influence of surface preparation of aluminum alloy AW-5754 and stainless steel x5crni18-10 on the properties of bonded joints. Materials 2024;17:2561. https://doi.org/10.3390/ma17112561.
[45] Li G, Lei M, Liang C, Li K, Li B, Wang X, et al. Improving adhesive bonding of Al alloy by laser-induced micro–nano structures. Appl Sci 2022;12:1199. https://doi.org/10.3390/app12031199.
[46] Çoban O, Bilgiç E, Akman E, Gümüş S. Laser treated novel textures for adhesion performance of aluminum alloy joints exposed to corrosion. Int J Adhesion Adhes 2024;132:103732. https://doi.org/10.1016/j.ijadhadh.2024.103732.
[47] Zhang C, Chen L, Zhang Y, Wang G, Jin J. Effect of laser processing microstructure on the bonding strength and failure mode of 7075-T6 aluminum alloy adhesive joints. J Manuf Process 2021;66:302–12. https://doi.org/10.1016/j.jmapro.2021.04.028.
[48] Freund J, Löbbecke M, Delp A, Walther F, Wu S, Tröster T, et al. Relationship between laser-generated micro- and nanostructures and the long-term stability of bonded epoxy-aluminum joints. J Adhes 2024;100:395–425. https://doi.org/10.1080/00218464.2023.2223475.
[49] Moroni F, Musiari F, Romoli L, Pirondi A. Influence of laser treatment parameters on the mode I strain energy release rate of aluminum double cantilever beam joints. Int J Adhesion Adhes 2018;83:31–40. https://doi.org/10.1016/j.ijadhadh.2018.02.023.
[50] Moroni F, Romoli L, Khan MMA. Design of laser-textured surfaces to enhance the strength of adhesively bonded joints. Int J Adhesion Adhes 2018;85:208–18. https://doi.org/10.1016/j.ijadhadh.2018.06.001.
[51] Moroni F, Musiari F, Pirondi A. Influence of laser ablation-induced surface topology on the mechanical behaviour of aluminium bonded joints. Proc Inst Mech Eng Part L J Mater Des Appl 2019;233:505–5202. https://doi.org/10.1177/1464420718813388.
[52] Moroni F, Musiari F, Favi C. Effect of the surface morphology over the fatigue performance of metallic single lap-shear joints. Int J Adhesion Adhes 2020;97:102484. https://doi.org/10.1016/j.ijadhadh.2019.102484.
[53] Samanta A, Huang W, Chaudhry H, Wang Q, Shaw SK, Ding H. Design of chemical surface treatment for laser-textured metal alloys to achieve extreme wetting behavior. ACS Appl Mater Interfaces 2020;12:18032–45. https://doi.org/10.1021/acsami.9b21438.
[54] Furlan V, Demir AG, Previtali B. Micro and sub-micron surface structuring of AZ31 by laser re-melting and dimpling. Opt Laser Technol 2015;75:164–72. https://doi.org/10.1016/j.optlastec.2015.06.030.
[55] Xie Y, Yang B, Lu L, Wan Z, Liu X. Shear strength of bonded joints of carbon fiber reinforced plastic (CFRP) laminates enhanced by a two-step laser surface treatment. Compos Struct 2020;232:111559. https://doi.org/10.1016/j.compstruct.2019.111559.
[56] Leone C, Paoletti A, Babu Yanala P, Lambiase F. Improving bonding strength of aluminium-PEEK hybrid metal-polymer joints by two-step laser surface treatment. Opt Laser Technol 2024;170:110304. https://doi.org/10.1016/J.OPTLASTEC.2023.110304.
[57] ASTM International. ASTM d1002-10 standard test method for apparent shear strength of single-lap-joint adhesively bonded metal specimens by tension loading (Metal-to-Metal). 2019. p. 1–6.
[58] MatWeb: Online Materials. Aluminum 6082-T6 n.d. https://www.matweb.com/search/DataSheet.aspx?MatGUID=fad29be6e64d4e95a241690f1f6e1eb7 (accessed December 9, 2024).
[59] Leone C, Genna S, Tagliaferri F. Multiobjective optimisation of nanosecond fiber laser milling of 2024 T3 aluminium alloy. J Manuf Process 2020. https://doi.org/10.1016/j.jmapro.2020.06.026.
[60] Lambiase F, Yanala PB, Leone C, Paoletti A. Repairing aluminum-PEEK hybrid metal-polymer joints made by thermo-mechanical joining. J Manuf Process 2023;93:1–14. https://doi.org/10.1016/J.JMAPRO.2023.03.018.
[61] Lambiase F, Yanala PB, Leone C, Paoletti A. Influence of laser texturing strategy on thermomechanical joining of AA7075 aluminum alloy and PEEK. Compos Struct 2023;315:116974. https://doi.org/10.1016/j.compstruct.2023.116974.
[62] Duflou JR, Sutherland JW, Dornfeld D, Herrmann C, Jeswiet J, Kara S, et al. Towards energy and resource efficient manufacturing: a processes and systems approach. CIRP Ann - Manuf Technol 2012;61:587–609. https://doi.org/10.1016/J.CIRP.2012.05.002.
[63] Apostolos F, Alexios P, Georgios P, Panagiotis S, George C. Energy efficiency of manufacturing processes: a critical review. Proced CIRP 2013;7:628. https://doi.org/10.1016/j.procir.2013.06.044.
[64] Leone C, Genna S, Caggiano A. Resource efficient low power laser cleaning of compact discs for material reuse by polycarbonate recovery. CIRP J Manuf Sci Technol 2015;9:39–50. https://doi.org/10.1016/j.cirpj.2015.01.005.
[65] Montgomery DC. Design and analysis of experiments. tenth ed. New York, NY: Wiley; 2019.
[66] Coleman DE, Montgomery DC. A systematic approach to planning for a designed industrial experiment. Technometrics 1993;53:1–12. https://doi.org/10.1080/00401706.1993.10484984.
[67] Romoli L, Moroni F, Khan MMA. A study on the influence of surface laser texturing on the adhesive strength of bonded joints in aluminium alloys. CIRP Ann 2017;66:237–40. https://doi.org/10.1016/J.CIRP.2017.04.123.
[68] Huntsman Corporation. The complete technical guide for adhesives - science and best practices. 2022.
[69] Griffo R, Di Natale F, Minale M, Sirignano M, Parisi A, Carotenuto C. Analysis of carbon nanoparticle coatings via wettability. Nanomaterials 2024;14:301. https://doi.org/10.3390/nano14030301.
[70] Williams JG, Morris CEM, Ennis BC. Liquid flow through aligned fiber beds. Polym Eng Sci 1974. https://doi.org/10.1002/pen.760140603.
[71] Meijer J. Laser beam machining (LBM), state of the art and new opportunities. J Mater Process Technol 2004;149:2–17. https://doi.org/10.1016/j.jmatprotec.2004.02.003.
[72] Semak V, Matsunawa A. The role of recoil pressure in energy balance during laser materials processing. J Phys D Appl Phys 1997;30:2541–52. https://doi.org/10.1088/0022-3727/30/18/008.
[73] Kaldos A, Pieper HJ, Wolf E, Krause M. Laser machining in die making - A modern rapid tooling process. J Mater Process Technol 2004;155–156:1815–20. https://doi.org/10.1016/j.jmatprotec.2004.04.258.
[74] Astarita A, Genna S, Leone C, Memola Capece Minutolo F, Squillace A, Velotti C. Study of the laser marking process of cold sprayed titanium coatings on aluminium substrates. Opt Laser Technol 2016;83:168–76. https://doi.org/10.1016/j.optlastec.2016.04.007.
[75] Jiang S, Zhang A, Zhan X, Hongyong J. Surface microtexturing design, laser-etching and adhesive failure of aluminum alloy single-lap-joint: experiment and simulation. Thin-Walled Struct 2023;193:111237. https://doi.org/10.1016/j.tws.2023.111237.
[76] Medjdoub SM, Madani K, Messid Y. Numerical analysis of the mechanical behavior on the effect of the geometric interface of the aluminum/aluminum plate assembly. Eurasia Proc Sci Technol Eng Math 2022;21:302–10. https://doi.org/10.55549/epstem.1226626.